NASA TN D-4711

EXPERIMENTAL STUDY OF VERTICAL IMPACTS OF AN LM-TYPE LANDING GEAR ASSEMBLY UNDER SIMULATED LUNAR GRAVITY

By John Locke McCarty and Huey D. Carden

Langley Research Center
Langley Station, Hampton, Va.

NATIONAL AERONAUTICS AND SPACE ADMINISTRATION

For sale by the Clearinghouse for Federal Scientific and Technical Information
Springfield, Virginia 22151 – CFSTI price $3.00

EXPERIMENTAL STUDY OF VERTICAL IMPACTS OF AN LM-TYPE LANDING GEAR ASSEMBLY UNDER SIMULATED LUNAR GRAVITY

By John Locke McCarty and Huey D. Carden
Langley Research Center

SUMMARY

An experimental study was made to evaluate the response of an LM-type landing gear system to simulated lunar landings on several penetrable target materials and to relate this response to that of penetrometers impacting the same materials. Testing included vertical impacts of a single landing gear unit at velocities up to approximately 3 m/sec. The test apparatus, designed to simulate the effects of lunar gravity on the landing gear unit, included a full-scale boilerplate pad and a vertical strut with stroking characteristics similar to those of LM (lunar module). The mass of the system approximated 25, 50, and 100 percent of the anticipated vehicle landing mass. The target materials consisted of two grades of quartz sand (one in a densely packed state) and an open cell urethane foam.

The results of this study show that the maximum anticipated accelerations sensed by the vehicle occupants and equipment would not exceed 3.3g (earth) in a vertical landing. During strut compression, which is intensified with increasing target bearing strength, with system mass and with impact velocity, these accelerations are shown to be a function of only the crushing strength of the collapsible strut and the system mass. Pad accelerations increase with increasing impact velocity and increasing target penetration resistance since both induce higher pad loading rates, and, during strut compression, are independent of the system mass. Data are presented which show that the penetration of the landing pad into particulate target materials can be reasonably estimated from the peak accelerations generated by penetrometers during impacts into the same target materials.

INTRODUCTION

The recent successful landings of the unmanned United States Surveyor and Russian Luna spacecraft on the surface of the moon have largely relieved earlier concern as to the capability of the lunar surface to support the Apollo lunar module (LM) during landing and to maintain the vehicle in a position suitable for subsequent operations. However, since the size, shape, loading, and design of the landing gear system of the manned vehicle

differ from those of the unmanned spacecraft, additional information is desired to enhance the reliability of LM landing systems. In addition, the LM landing site will be removed, if only by several meters, from Surveyor and Luna landing positions. Thus, a knowledge of the response of the LM gear during impacts upon materials similar to those which might possibly be encountered on the surface of the moon is of vital importance to the Apollo program and has prompted much research in the field.

The touchdown stability of lunar landing vehicles on impenetrable surfaces, including a dynamically scaled LM, has been investigated experimentally and analytically in references 1 to 3, among others. References 4 and 5 describe the apparatus and some results from drag and impact tests performed on penetrable materials with both sub- and full-scale LM pads to obtain data which would permit the development of expressions for predicting the response of LM during a lunar landing. However neither the LM mass nor the lunar gravitational effects are being simulated in the full-scale pad tests. The predicted pad penetrations of LM based upon the dynamics of the Surveyor 1 landing are given in reference 6, but this computer study considered only vertical landings upon an incompressible soil model.

In view of the need for supplementary information to support dynamic analyses of full-scale LM landings, an experimental study was made of an LM-type landing gear assembly impacting penetrable targets. Testing was limited to vertical impacts of a single landing gear unit at velocities up to approximately 3 m/sec. The test apparatus, designed to simulate the effects of lunar gravity on the landing gear unit, included a full-scale boiler plate pad and a vertical strut with stroking characteristics approximating those of LM. This experimental study was part of a recent penetrometer impact research program conducted for NASA by the Aeronutronic Division of the Philco Corporation and discussed in references 7 to 9. The results of this study and a correlation between landing gear response characteristics and the response of penetrometer impacts on the same target materials are presented in this report. Considerable information, including photographs, has been extracted from references 7 and 9 which present portions of the test results.

APPARATUS

An artist' s sketch of the test facility constructed for performing the impact tests with the simulated LM landing gear unit is given in figure 1. This facility consisted of the movable gantry, which supported the simulated LM test assembly, and the pits which served as target material reservoirs. Details of the test assembly and its instrumentation and a description of the materials selected for targets are discussed in the paragraphs which follow.

Test Assembly

A sectional view of the major components of the simulated LM test assembly are identified in figure 2. These components include a rigid pad, a vertical telescoping strut with stroke characteristics equivalent to those designed for LM, sufficient ballast to duplicate the LM mass, and a pneumatic lunar-gravity simulator which simulated the effects of lunar gravity on the impacting system.

Figure 3 shows a sketch of the test pad together with a curve which relates the pad bearing (cross-sectional) area to the penetration depth. The pad duplicated the LM dimensional configuration but was constructed of cast aluminum instead of fiber glass and honeycomb. The pad had a maximum diameter of 94 cm, a height of 17.8 cm, and a mass of 52.2 kg. As shown in figure 3, the contour of the pad bearing surface was composed of a central surface with a radius of 127 cm which blended near the rim into a surface with a 15.24-cm radius of curvature.

The pad was rigidly attached to a strut consisting of a vertical member which, as shown in figure 2, telescoped into a cylinder containing crushable honeycomb cartridges. The two precrushed honeycomb cartridges had different loading and stroking characteristics. One cartridge was 43.6 cm long and designed to crush at a constant force of 26.7 kN for 70 percent of its original length and the other, 72.4 cm long, was designed to crush at a constant force of 53.4 kN over 70 percent of its original length. The results of a static loading test and a typical dynamic test performed on two sets of honeycomb cartridges are presented in figure 4. The figure shows that in both tests, the strengths of the cartridges slightly exceeded their design strengths and that the weaker cartridge stroked further than anticipated. The values for the test honeycomb strength (26.7 and 53.4 kN) were selected in mid-1965 based upon the LM design as it then existed and are somewhat greater than the current values of 20 and 42.2 kN as quoted in reference 10. However, the weaker main strut on LM is inclined to the vertical approximately 26.5° and is supported by horizontal secondary struts. Thus, characteristics of the strut for the tests described herein appear to reasonably approximate those for the LM strut.

Ballast, in the form of steel blocks each with a mass of 1814 kg, was incorporated into the test assembly to provide total masses approximating 25, 50, and 100 percent of the LM mass which represented upper bounds for pad loadings for a four-, two-, and one-leg impact landing condition, respectively. As shown in figure 2, this ballast was rigidly attached to the strut below and suspended during operation from the lunar gravity simulator.

The lunar gravity simulator consisted of a cylinder vented at the bottom to a large tank of compressed air which applied a constant force to a piston which was engaged by the free-falling LM assembly prior to pad impact. The air pressure was preset to provide a resistance force equal to 5/6 of the earth weight of the LM assembly. Thus, as

the pad impacted the target, the weight of the LM assembly was reduced to 1/6 of the earth value while retaining the full inertial mass properties. This simulator had a stroke capability of over 1.8 m and could handle up to approximately 7300 kg.

Target Materials and Preparation

Targets for this investigation were selected from those employed in the penetrometer research program and included two grades of quartz sand and an open cell urethane foam. The sands consisted of Nevada 60 which had a mean grain size of 160 μ and Nevada 120 with a mean grain size of 70 μ. The detail characteristics of these sands are defined in references 7 and 8. The Nevada 60 sand, tested in a loosely packed state, had a nominal in situ density of 1558 kg/m^3 and the Nevada 120 sand was tested under two packing conditions: dense (nominal density of 1506 kg/m^3) and loose (nominal density of 1378 kg/m^3). The urethane foam had a density of 32 kg/m^3 and was in the form of 25-cm-thick molded units. The sands were placed in approximately 4.6-m square pits to a depth of roughly 1.5 m and the urethane foam units were stacked to approximately the same depth in the smaller pit shown in figure 1.

The state of compaction of the sand targets was made repeatable from test to test by means of an aerification technique similar to that successfully employed in the penetrometer program (refs. 7 and 8). This technique consisted of forcing gaseous nitrogen up through the target materials from orifices drilled in an array of pipes positioned on the floor of the pits. These pipes were covered with a felt pad which diffused the gas and also prevented the sands from clogging the orifices. The aerification technique which produced the loosely packed state in the sands was employed prior to each test. The dense state of the Nevada 120 sand was attained by controlled insertions of a concrete vibrator into the sand following the aerification process.

The target materials were examined for their resistance to quasi-static loadings or bearing strength. The apparatus for performing these tests, movable to permit testing at any location in the pit, is pictured mounted to the gantry in figures 1 and 2 and consisted of a hydraulic cylinder with a load capability of nearly 72 kN and a stroke of approximately 64 cm. Probes which included 21.6- and 30.5-cm-diameter spheres, a 21.6-cm-diameter disk and the test pad were forced into each target material (exception: the disk in the dense Nevada 120 sand) at a rate of 2.5 cm/min to a depth of approximately 60 cm or to a maximum load of 71 kN. The probes other than the pad were selected to correspond to the dimensions of penetrometers which were impact tested in these materials. The results of these probe tests are given in figures 5 and 6 where the loading divided by the projected penetration area (area in the plane of the original surface at each penetration) of each probe is presented as a function of the probe penetration depth. Also included in the figure for the sands are the results from a small 6.35-cm-diameter spherical probe

which served as a standard and was employed prior to every test in sand to assure that the target material had been satisfactorily prepared. The results from four such tests are presented to illustrate the extent of scatter noted for each sand target. These "standard" tests were performed with a lower capacity motor-driven unit having a constant penetration rate of 1.27 cm/sec.

Instrumentation

The instrumentation for monitoring the LM landing gear impact tests consisted of load cells, accelerometers, and displacement potentiometers with attendant signal conditioning and recording equipment. The locations of the monitoring instruments on the test support structure are identified in the sketch of figure 7. Load cells were mounted between the pad and strut and to the rod which extended from the piston in the lunar gravity simulator. Both the ballast and the test pad were equipped with accelerometers, and the displacement sensors were attached to measure strut stroking and the distance of ballast travel. The outputs from all sensors were recorded on an oscillograph recorder. A typical record from an impact test is reproduced in figure 8.

TEST PROCEDURE

The test technique consisted of impacting the simulated LM landing gear assembly onto the targets of prepared sand beds and urethane foam and recording the measured impact characteristics. Preparation of the sand targets involved application of the aerification technique to obtain the desired material consistency as verified by subsequent quasi-static probe tests. All targets were impacted at a nominal velocity of 3.05 m/sec since landing criteria for LM specify that as the maximum vertical impact velocity. Additional tests at nominal impact velocities of 0.9 and 2.1 m/sec were performed on the sand targets. All velocities were obtained by means of the gravity-drop principle wherein the pad, strut, and simulated mass were released at a height above the target surface corresponding to the desired impact velocity. Release was accomplished by firing explosive bolts (fig. 2) which severed the coupling between the impacting system and the gantry directly below the lunar-gravity simulator. The gravity simulator was engaged by the free-falling apparatus just prior to pad contact with the target material and provided a constant force equal to approximately 5/6 of the earth weight of the apparatus throughout the remainder of the system motion. The instrumentation provided dynamic data of displacements, accelerations, and forces which were incurred during the impact process. Following each test, the recorded displacements were verified by physical measurements of the pad penetration and the strut stroke. The impacting system was elevated for the succeeding test by increasing the air pressure in the lunar gravity simulator tank which applied an upward force to the internal piston. In addition to serving as a housing for the

gravity simulator load cell and the engaging link for the free-falling system, the rod which extended from this piston served as a guide to the impacting simulated LM assembly.

Sufficient ballast was added to the impacting system to provide total masses approximating 25, 50, and 100 percent of the LM mass which represented upper bounds for pad loadings for four-, two-, and one-leg landing impact conditions, respectively.

PRESENTATION OF DATA

Data from the simulated LM impact tests were obtained from records similar to the one reproduced in figure 8, which display the outputs from the various sensors attached to the impacting system. These records, either directly or indirectly, provided information which permitted the following simulated lunar impact time-history characteristics to be calculated: pad and lunar gravity simulator loadings (or forces), pad and ballast accelerations, ballast displacement with respect to the target surface, strut stroking, and pad penetration into the target material. Impact-data time histories which were obtained from all tests are presented in figure 9 where the signals, particularly those from the accelerometers, have been faired. The displacements and accelerations are presented as obtained from the test records; however, the measured lunar gravity simulator force is presented in ratio form – divided by the desired force of 5/6 of the earth weight of the impacting system. In addition, to serve as a check on the instrumentation, the recorded LM pad loading is accompanied by the loading as calculated at various time intervals on the basis of the measured ballast accelerometer data and the corresponding lunar gravity simulator force. LM pad testing in the sands consisted of impacting the 1715-kg and 3506-kg masses at nominal velocities of 0.9, 2.1, and 3.05 m/sec and the 6845-kg mass at the nominal 3.05 m/sec. Tests on urethane foam (figs. 9(v), 9(w), and 9(x)) were limited to the nominal impact velocity of approximately 3 m/sec since it was apparent that this target (crushing strength of approximately 200 kN/m^2) was sufficiently strong to support the LM vehicle under the most severe vertical landing test condition of the system.

DISCUSSION OF RESULTS

Figure 9 shows that, in general, the force applied by the simulator agrees favorably with that required to simulate lunar gravity forces on the landing gear. Furthermore, this restraining force is shown to be generally maintained throughout the duration of each test. The figure also shows the agreement between the measured LM pad loading (or force) and that calculated from the response of the ballast accelerometer and the simulator load cell (see appendix), which indicates satisfactory performance of the

instrumentation. On the basis of realistic lunar gravity simulation and adequately performing instrumentation, significant features of the data of figure 9 are compiled in figures 10 to 13 to illustrate the response of the LM system to various loading conditions and to target materials of different penetrability characteristics.

Pad Forces

Figure 10 illustrates a typical variation in the time history of the force applied to the test pad with system momentum resulting from different impact velocities. As shown in the appendix, this force is essentially the same as the force exerted by the soil since the mass of the pad is relatively low. For the time histories shown, the mass of the system is 3506 kg and the target is loosely packed Nevada 120 sand. The figure shows that from the onset of impact the force increases until reaching levels which correspond to those necessary to crush the honeycomb cartridges within the strut. The rate of increase of the applied force is dependent upon the impact velocity – the higher the velocity, the shorter the time required to initiate strut stroking. At the two lower impact velocities only the 26.7-kN honeycomb underwent crushing whereas at the highest velocity this cartridge was completely stroked and some crushing occurred in the 53.4-kN honeycomb. The trend of the data of this figure is similar to that for other values of system mass and for other targets; however, in some tests (low mass and low velocity) no honeycomb crush was detected while in others (high mass and high velocity) the stroking limit of both honeycomb cartridges was reached and pad forces in excess of 53.4 kN were measured. The dip which exists early in the illustrated force time history at 2.35 m/sec and noted in other tests of figure 9 is consistent with acceleration time histories of penetrometer response at low impact velocities in similar target materials (refs. 10 and 11).

Pad Penetrations

The resulting penetration depths of the test pad into each of the sand targets are summarized in figure 11 as a function of impact velocity for the different system masses. Also denoted in the figure are the maximum pad penetrations recorded for those tests wherein pad rebound occurred. Targets are arranged on the figure in the order of their penetration resistance or bearing strength – loose and packed Nevada 120 sands being the weakest and most resistant, respectively. The figure shows that, at corresponding impact conditions (system mass and impact velocity), pad penetration in sands decreases with increasing target bearing strength. The data of figure 9 show that this trend also encompasses the penetration into urethane foam with the exception of the 3506-kg mass at 3.05 m/sec.

The variation of pad penetrations with both impact velocity and system mass appears to be dependent upon the target. In the loose Nevada 120 sand, pad penetration

increases with increasing velocity over the test velocity range whereas, in the less penetrable Nevada 60 and packed Nevada 120 sands, penetrations reach a maximum at a velocity of approximately 2 m/sec. Similarly, pad penetration in all targets except the packed Nevada 120 sand generally increases with increasing system mass. Figure 11 shows that pad penetration in the packed Nevada 120 sand is less for a system mass of 3506 kg than that for 1715 kg for all test velocities. The relatively deep penetrations associated with the 6845-kg mass impacting all targets can be attributed to the bottoming of the honeycomb cartridges within the strut which meant that forces in excess of 53.4 kN were applied to the pad.

Strut Compression

The extent of strut compression for each of the impact tests in the different sands is summarized in figure 12. The average stroking limit of the weaker honeycomb cartridge is identified in the figure and conditions in which both cartridges bottom out are noted. Again, the targets are arranged on the figure in the order of their penetration resistance. The figure shows that, for test conditions where strut compression occurs, the amount of compression increases with increasing target bearing strength, system mass, or impact velocity. The strut compression associated with impacts onto urethane foam (figs. 9(v), 9(w), and 9(x)) are somewhat less than that of the lower bearing strength, packed Nevada 120 sand for corresponding impact conditions. This variance in the trend of the data may be attributed to differences in the failure modes of the two targets. The data of figure 12 and those for the urethane foam also show that, for conditions where the system mass was 6845 kg and the impact velocity was approximately 3 m/sec, the stroking limit of both honeycomb cartridges was reached on all targets; whereas, for a system mass of 1715 kg, strut compression was limited to only the 26.7-kN honeycomb cartridge.

System Accelerations

The maximum accelerations sensed by the test pad and the ballast during impact of the system with the sand targets are summarized in figure 13. The accelerations are presented as a function of impact velocity for the different system masses and the targets are arranged on the figure in the order of increasing penetration resistance. The maximum pad accelerations are given in figure 13(a) and the ballast accelerations, which would correspond to those sensed by the occupants and equipments within the vehicle, are given in figure 13(b). As shown in figure 9 and as observed through a comparison of figures 13(a) and 13(b), the peak accelerations of the pad and the ballast are effectively the same for tests involving no strut compression. This agreement was expected since, with no strut compression, these two components of the system are essentially rigidly attached and, as such, would sense identical accelerations.

The peak accelerations of the pad for impacts which involve strut compression are shown for the different targets in figure 13(a) to increase with increasing impact velocity and to be essentially independent of the system mass. During compression, the force on the pad is equal to that force required to crush the honeycomb cartridges which is irrespective of the mass of the impacting system. However, the impact velocity affects the peak acceleration since the velocity regulates the rate at which the force is applied to the pad – the higher the loading rate, the greater the acceleration. Figure 13(a) further shows that, for similar impact conditions, the peak acceleration sensed by the pad increases with the penetration resistance of the target material. With targets of increased strength, the force on the pad equals that required to induce strut compression at shallower pad penetrations and, hence, at correspondingly higher loading rates which account for the increased peak accelerations.

As noted in figure 9, the variation of the ballast accelerations with time is in accord with the time histories of the pad loadings. These ballast accelerations can be computed by relating the force, which is equal to the pad loading, to the ballast mass. Hence the ballast accelerations are a maximum when the pad loading is greatest. Furthermore, during strut compression, where the force is defined by the crushing strength of the honeycomb cartridges, the ballast accelerations would be anticipated to be a function of only the ballast mass. Figure 13(b) shows that, as predicted, the ballast accelerations associated with the crushing of each honeycomb cartridge for a given system mass (the extent of strut compression is noted in the figure) are essentially invariant with the impact velocity and the target penetration resistance. These accelerations are in good agreement with those calculated from a knowledge of the crushing strength of the stroked honeycomb cartridges. For example, the calculated acceleration based upon a system mass of 3506 kg (ballast mass is 3449 kg) stroking the 26.7-kN cartridge is 0.78g and the experimental data for this condition range between 0.55g and 0.80g. Similar agreement is noted for other test conditions including impacts on urethane foam.

No predictions can be made as to the accelerations generated when the strut bottomed out. However, strut bottoming occurred only when the system mass was a maximum (6845 kg), which corresponded to an impact landing solely on one leg. Such a landing would be extremely rare since other legs would contact the surface during the landing process and absorb some of the vehicle impact energy. Thus, since the ballast accelerations are inversely proportional to the system mass, it appears reasonable to assume that the maximum expected accelerations sensed by the occupants and equipment of a vehicle landing at 3.05 m/sec or less, employing a strut similar to that described herein, would not exceed 3.3g (1715-kg mass during crush of the 53.4-kN honeycomb cartridge).

Correlation of LM Pad and Penetrometer Test Results

One of the objectives of this research program was to correlate the results of the simulated landing gear tests with penetrometer impact test data. Of specific interest is the ability of the penetrometer to predict the depth to which a subsequently landing LM-type vehicle will penetrate a surface. The data of reference 8 showed that penetrometers are capable of identifying the nature of the impacted surface – that is, whether the surface is rigid, or is composed of a weakly bonded material which has a collapsible failure mode (urethane foam, for example), or consists of particulate materials which fail in compression. It is further shown in the reference that penetrometer information, particularly peak impact accelerations, can distinguish between particulate materials of different bearing strength – the greater the bearing strength, the higher the peak acceleration. Surfaces which are identified by penetrometers as being either rigid or having a collapsible failure mode pose no problems to predictions of landing pad penetrations. Little or no penetration would occur in the rigid surface, and pad penetrations into the latter can be estimated from the material crushing strength which, as discussed in reference 8, can be readily computed from the penetrometer data. However, pad penetration into particulate materials which fail in compression, such as sands, is unpredictable without experimental testing because of the complex nature of the structural failures of these materials. Hence, the testing discussed in this paper was devoted primarily to this target class.

Figure 14 summarizes the pad penetrations in the particulate targets of this program as a function of the ratio of the system energy at impact to the overall pad area. The symbols represent the test points which are faired by the solid curves. Also indicated by the dashed lines in the figure are the approximate penetration depths at which the soil resistance is sufficiently large to initiate compression in the strut honeycomb cartridges. The figure shows that, as the penetration resistance or bearing strength of the target is decreased, this force, as expected, is developed at deeper penetration depths. The figure also shows that pad penetration following the onset of strut compression is small since the remaining impact energy is being absorbed in stroking the strut. Hence, at a given energy level, particularly in the upper range, there is a clear distinction between the pad penetration depths into the three targets examined.

A graphical relationship between penetrometer data and pad penetrations for these targets is given in figure 15 where the targets are further described by a relative bearing strength as defined in reference 8. This figure relates the peak impact accelerations sensed by the penetrometer considered to be of nominal design for the Apollo mission to the penetration of an LM pad during a vertical (1715 kg) landing. The penetrometer data, taken from reference 8, were obtained at an impact velocity of approximately 46 m/sec and the pad impact velocity was approximately 3 m/sec. Also included in the figure are

the penetrometer data from an impact with a rigid plate where no pad penetration would occur. The figure shows that particulate targets of decreasing bearing strength yield deeper pad penetrations and lower penetrometer peak accelerations and thereby suggests that penetration of the pad into a remote surface can be estimated from information previously obtained from penetrometers impacted upon that same surface. However, the figure also shows that for changes in the target bearing strength, pad penetrations are much more sensitive than the penetrometer response. A small variation in the bearing strength of these targets is reflected in a similar variation in penetrometer response and, in general, a much greater variation in pad penetration. The relationship illustrated in figure 15 is appropriate to the particulate targets of this paper; other targets, particularly those possibly critical to an LM landing, would require similar penetrometer and LM pad testing to provide a useful correlation.

CONCLUDING REMARKS

An experimental study was made to evaluate the response of an LM-type landing gear system to simulated lunar landings on several penetrable target materials and to relate this response to that of penetrometers impacting the same materials. Data are presented for system masses which approximated 25, 50, and 100 percent of the anticipated vehicle landing mass impacting at vertical velocities up to approximately 3 m/sec. The data are in the form of time histories which included pad and strut displacements, pad loading, and pad and ballast accelerations, all of which were measured during the impact process. An analysis of these data suggests the following remarks.

During landing, the loading on the pad, which essentially is the same as the resistance force developed in the target material, increases until it reaches a level which corresponds to that necessary to crush the honeycomb cartridges within the strut. The rate of increase of the loading is dependent upon the impact velocity – the higher the velocity, the shorter the time required to initiate strut stroking. For landing conditions which result in little or no strut compression, the loading time history is similar to that exhibited by penetrometers on such targets. For conditions involving strut compression, the force on the pad is equal to that required to crush the honeycomb cartridges, which is irrespective of the system mass. Thus, peak accelerations of the pad during strut compression are independent of the system mass, but do increase with increasing impact velocity and increasing target penetration resistance since both induce higher pad loading rates. However, the ballast accelerations, which correspond to the accelerations sensed by the vehicle occupants and equipment, are dependent only upon the system mass during strut compression.

The likelihood of one or two legs absorbing all of the system energy during landing of the vehicle appears to be remote since other legs would probably contact the surface

during the landing process. Thus, strut bottoming is improbable and the maximum anticipated accelerations sensed by the main body of the vehicle (ballast), based upon a strut having characteristics similar to those employed in these tests, would not exceed 3.3g (earth).

The penetration of the landing pad into particulate materials can be reasonably estimated from the peak accelerations generated by penetrometers during impacts into the same materials. Particulate targets of decreasing bearing strength yield deeper pad penetrations and lower penetrometer peak accelerations. However, for changes in the target bearing strength, pad penetrations are much more sensitive than the penetrometer response. A small variation in the bearing strength of these targets is reflected in a similar variation in penetrometer response and, in general, a much greater variation in pad penetration.

Langley Research Center,
National Aeronautics and Space Administration,
Langley Station, Hampton, Va., May 22, 1968,
124-08-05-15-23.

APPENDIX

EQUATIONS OF MOTION FOR THE IMPACTING TEST SYSTEM

A simple representation of the forces involved during impact of the test apparatus is given in the sketch. These forces include

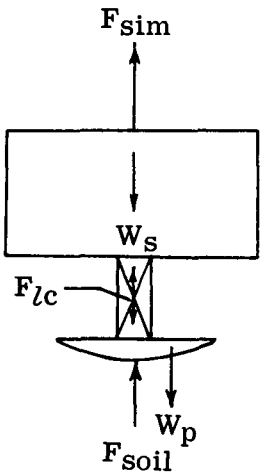

W_s	weight of ballast and strut
W_p	weight of test pad
F_{sim}	force exerted by simulator
F_{soil}	force exerted by soil
F_{lc}	force measured by load cell

The force measured by the load cell is the pad loading and can be calculated from the known or measured forces either above or below the load cell. Considering those forces above the cell, the dynamic equation of equilibrium is

$$F_{lc} + F_{sim} - W_s = W_s A_s$$

where A_s is the acceleration of the ballast and strut in earth g units. Thus,

$$F_{lc} = W_s(A_s + 1) - F_{sim}$$

which is the calculated pad loading referred to in figure 9.

The soil force can be obtained from the following equation of motion developed from the forces below the load cell:

$$F_{soil} - F_{lc} - W_p = W_p A_p$$

where A_p is the acceleration of the test pad in earth g units. Thus,

$$F_{soil} = F_{lc} + W_p(A_p + 1)$$

which states that the force exerted by the soil is slightly greater than the pad loadings of figure 9.

REFERENCES

1. Donroe, F.: Results of Landing Gear Stability Drop Tests 1/6 Scale Model. Rep. No. LTR 904-16001 (Contract No. NAS 9-1100), Grumman Aircraft Eng. Corp., Sept. 6, 1963.

2. Walton, William C., Jr.; and Durling, Barbara J.: A Procedure for Computing the Motion of a Lunar-Landing Vehicle During the Landing Impact. NASA TN D-4216, 1967.

3. Herr, Robert W.; and Leonard, H. Wayne: Dynamic Model Investigation of Touchdown Stability of Lunar-Landing Vehicles. NASA TN D-4215, 1967.

4. Anon.: Mid Term Report of Lunar Module (LM) Soil Mechanics Study. Rep. No. MM-67-2 (NASA Contract No. NAS 9-5759), Bendix Corp., Jan. 26, 1967.

5. Black, R. J.; and Winters, H. K.: A Semiempirical Model for Prediction of Soil Reactive Forces and Footpad Penetrations for Spacecraft Landings. ECD No. AM-67-3 (Contract No. NAS9-5759), Bendix Corp., June 1967.

6. Shipley, E. N.: Surveyor and LM Penetration in a Model Lunar Soil. TM-67-1014-1, Bellcomm, Inc., Feb. 23, 1967.

7. Anon.: Final Report – Research, Development, and Preliminary Design for the Lunar Penetrometer System Applicable to the Apollo Program. Publ. No. U-3556 (Contract No. NAS1-4923), Aeronutronic Div., Philco Corp., Apr. 27, 1966.

8. McCarty, John Locke; and Carden, Huey D.: Response Characteristics of Impacting Penetrometers Appropriate to Lunar and Planetary Missions. NASA TN D-4454, 1968.

9. Anon.: Final Report – Research, Development, and Preliminary Design for the Lunar Penetrometer System Applicable to the Apollo Program. Publ. No. U-3608 (Contract No. NAS1-4923), Aeronutronic Div., Philco Corp., June 3, 1966.

10. McCarty, John Locke; and Carden, Huey D.: Impact Characteristics of Various Materials Obtained by an Acceleration-Time-History Technique Applicable to Evaluating Remote Targets. NASA TN D-1269, 1962.

11. Hanks, Brantley R.; and McCarty, John Locke: Investigation of the Use of Penetrometers To Determine the Capability of Dust Materials To Support Bearing Loads. NASA TN D-3200, 1966.

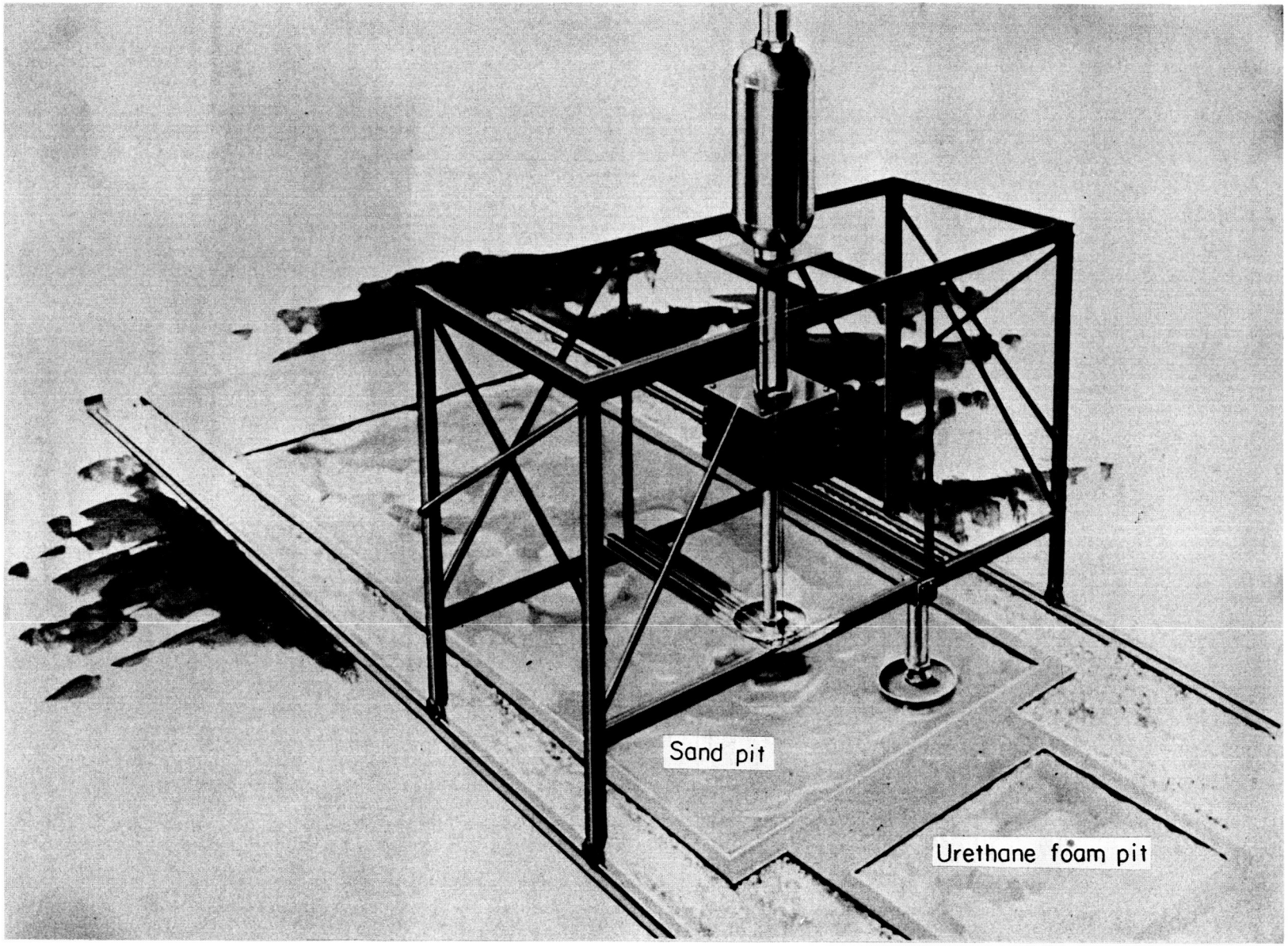

Figure 1.- Artist's sketch of test facility.

L-68-895

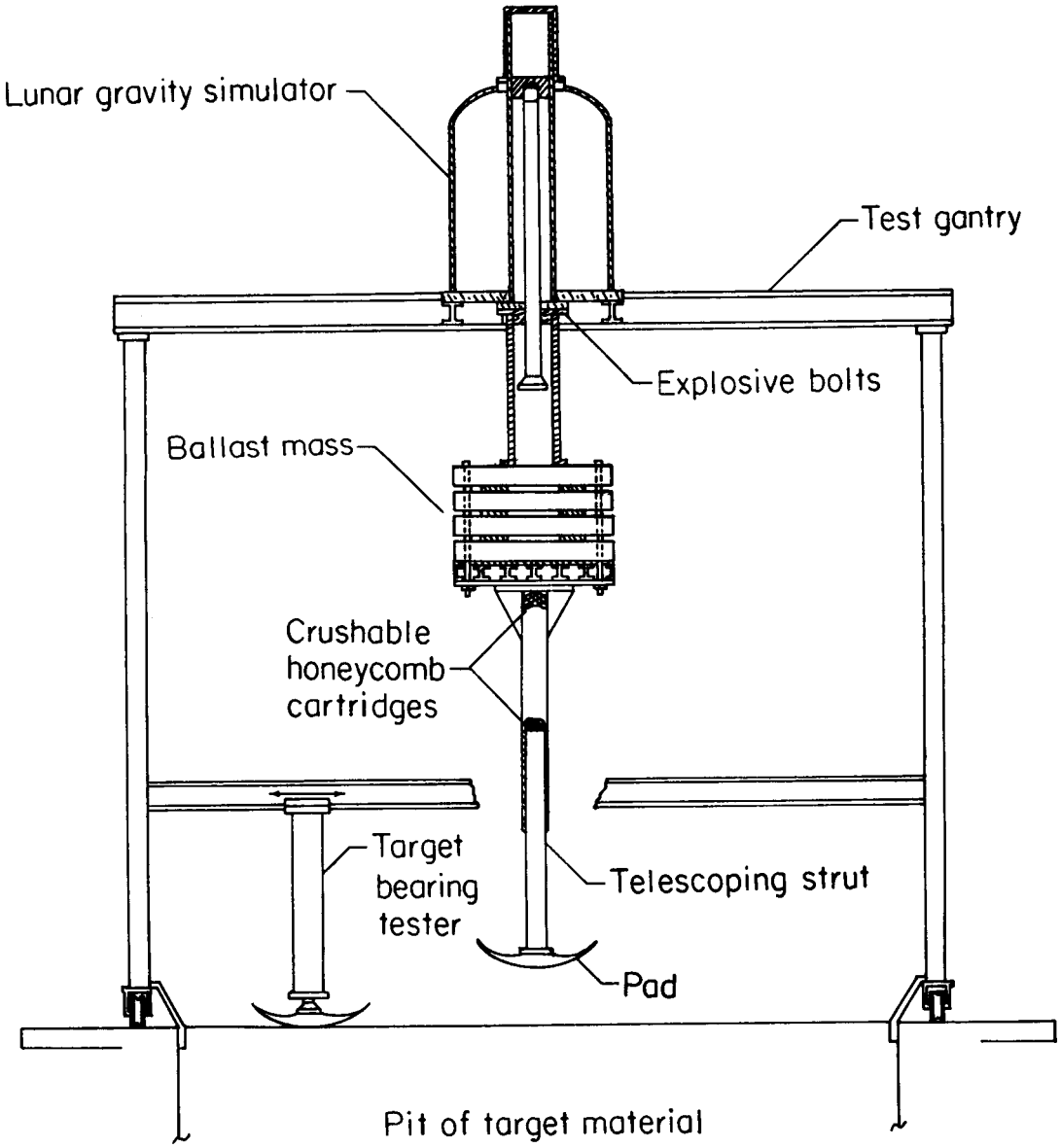

Figure 2.- Test assembly showing major components.

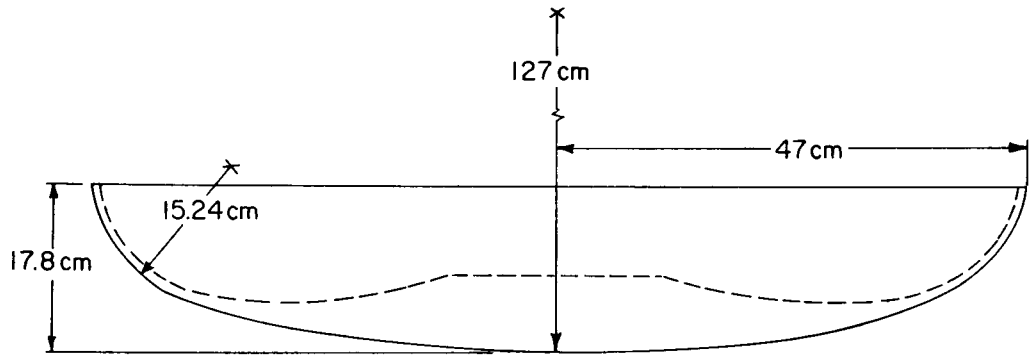

(a) Test pad.

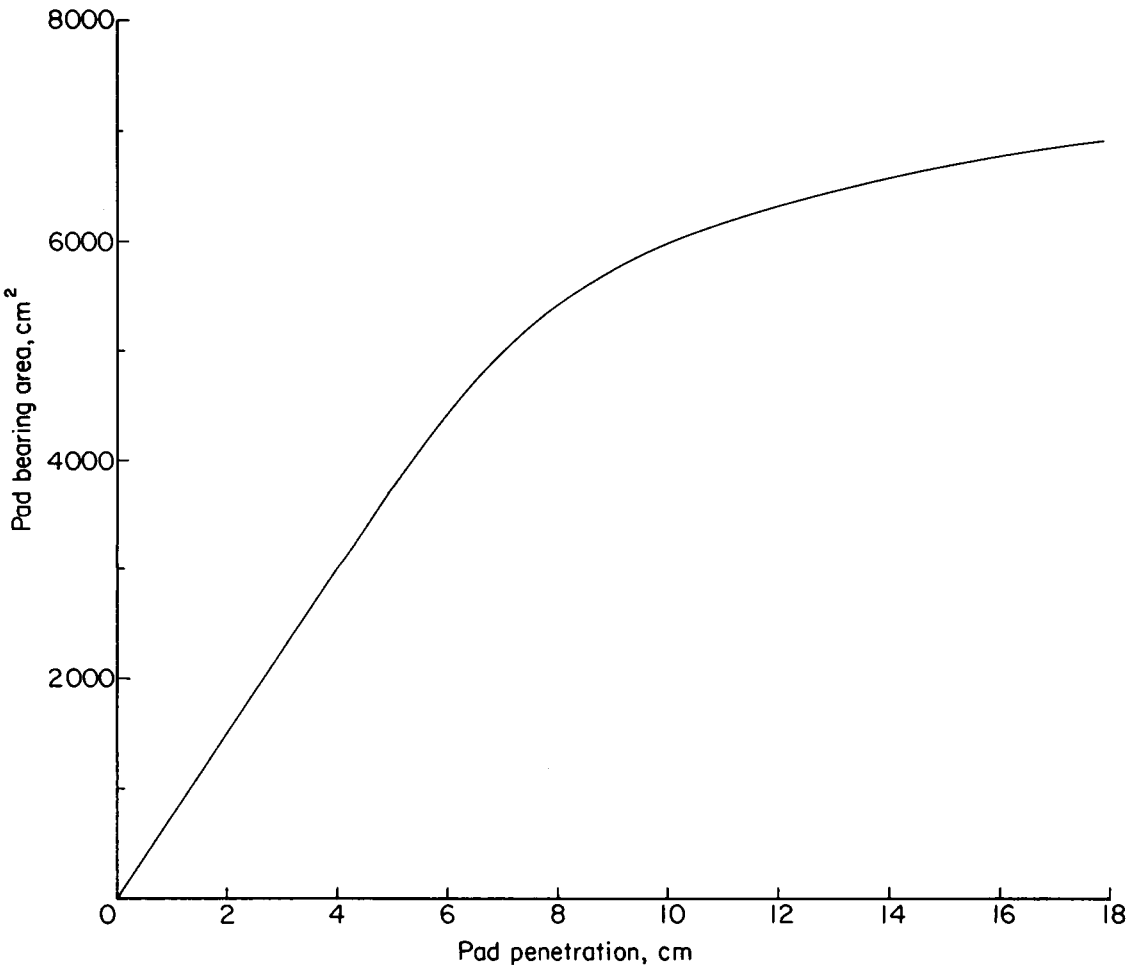

(b) Variation of pad bearing area with penetration.

Figure 3.- Physical characteristics of test pad.

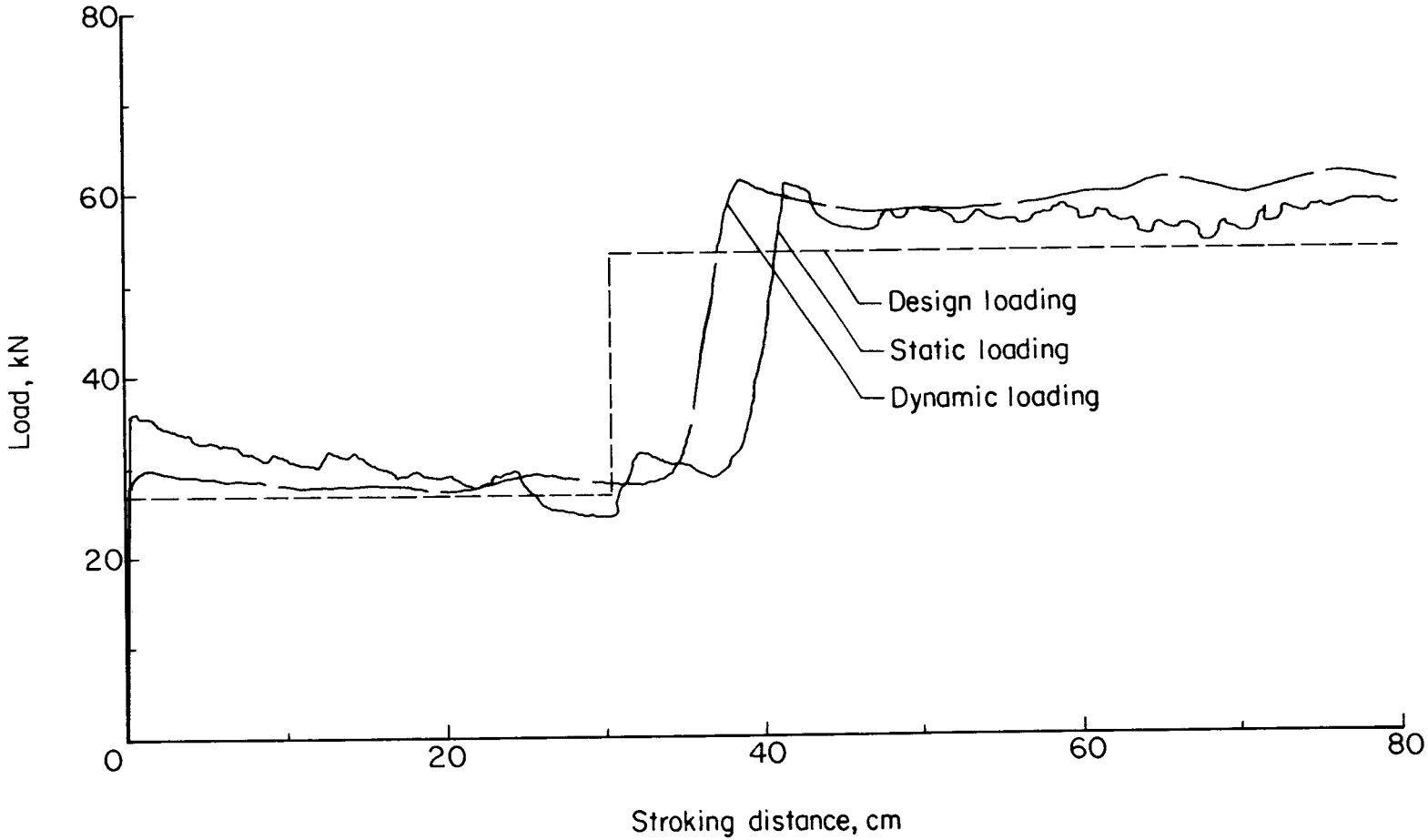

Figure 4.- Results of static and typical dynamic loading of honeycomb cartridges employed within the collapsible strut.

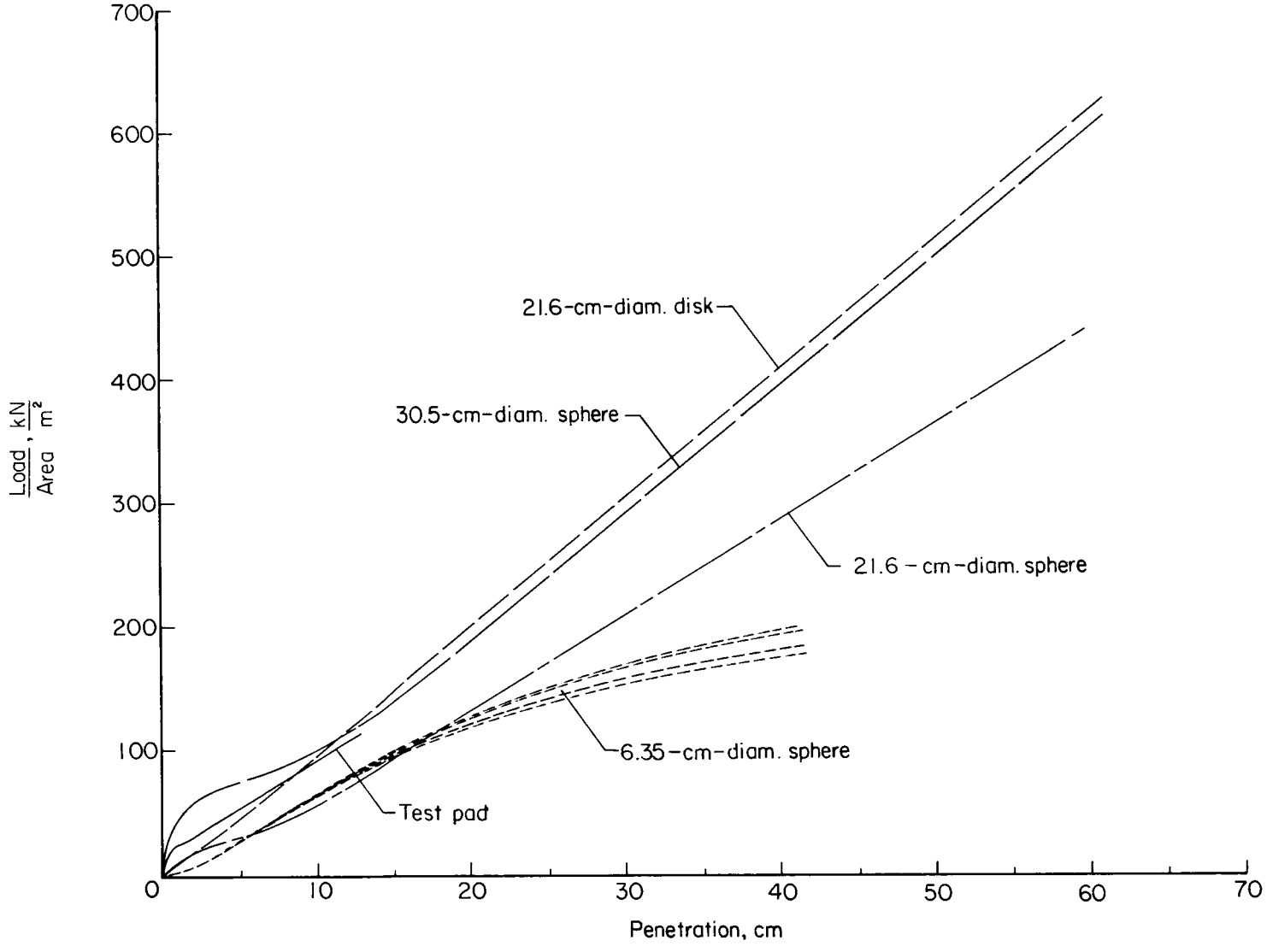

(a) Loosely packed Nevada 60 sand.

Figure 5.- Results from quasi-static loading tests performed on test target materials.

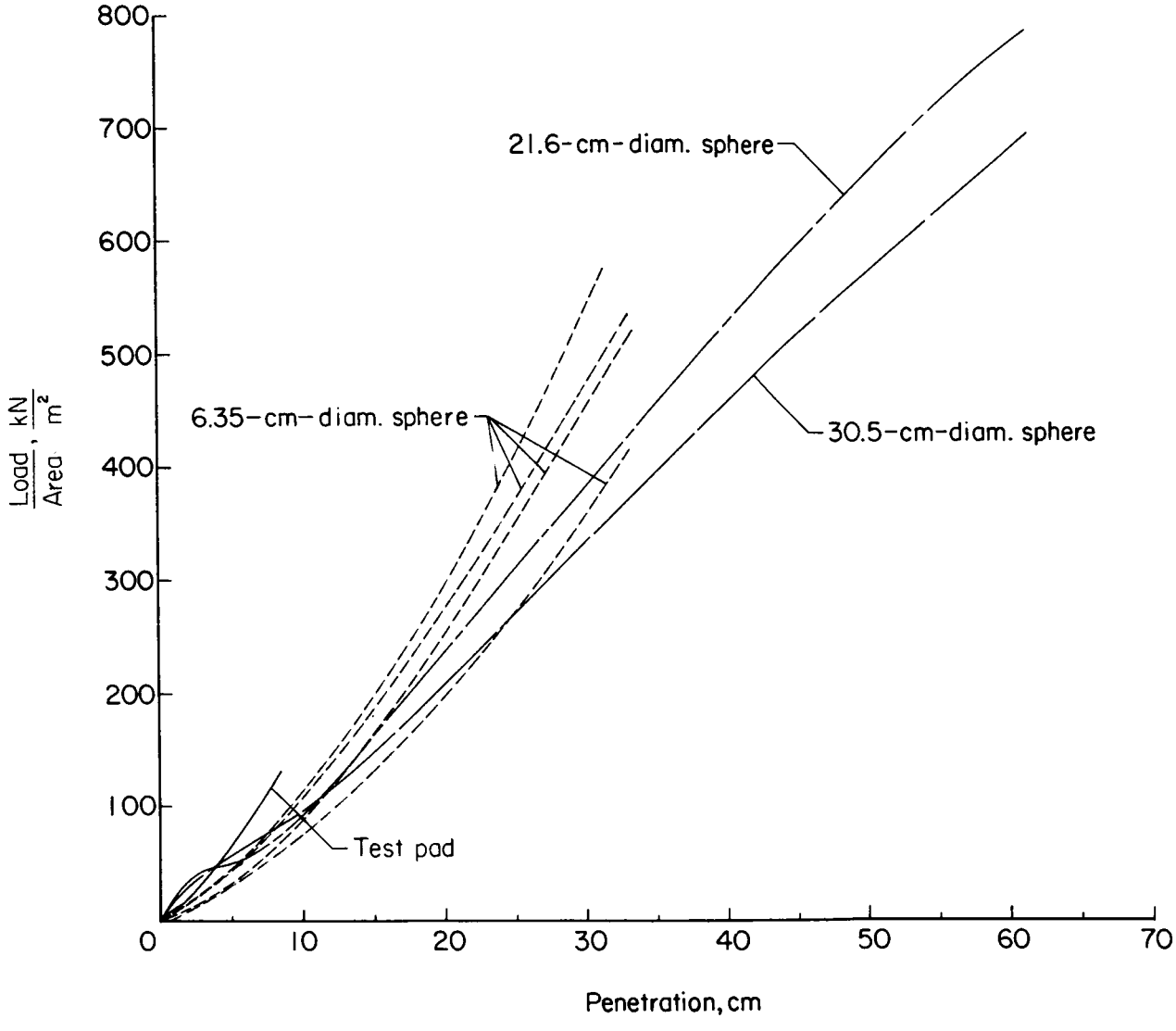

(b) Densely packed Nevada 120 sand.

Figure 5.- Continued.

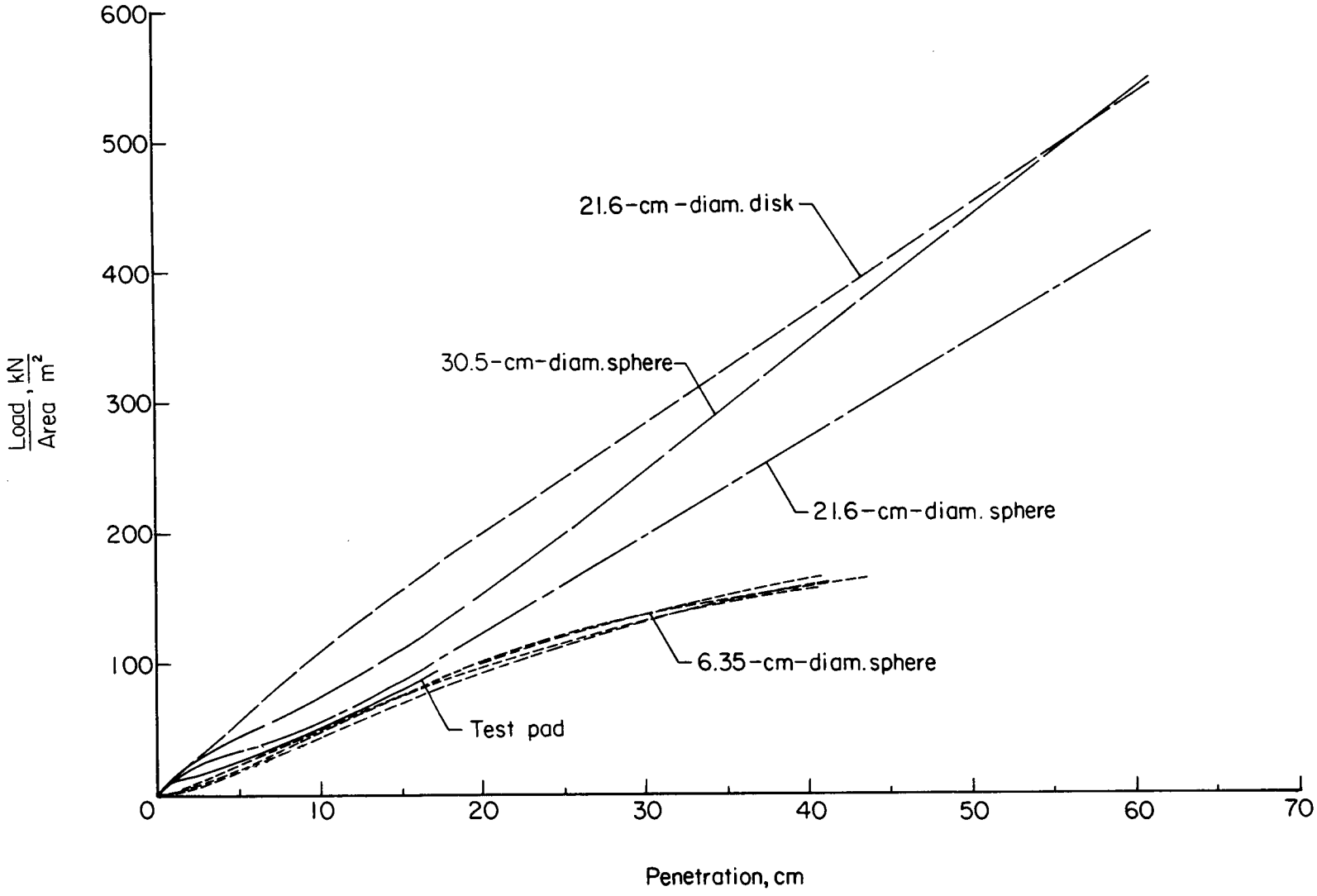

(c) Loosely packed Nevada 120 sand.

Figure 5.- Continued.

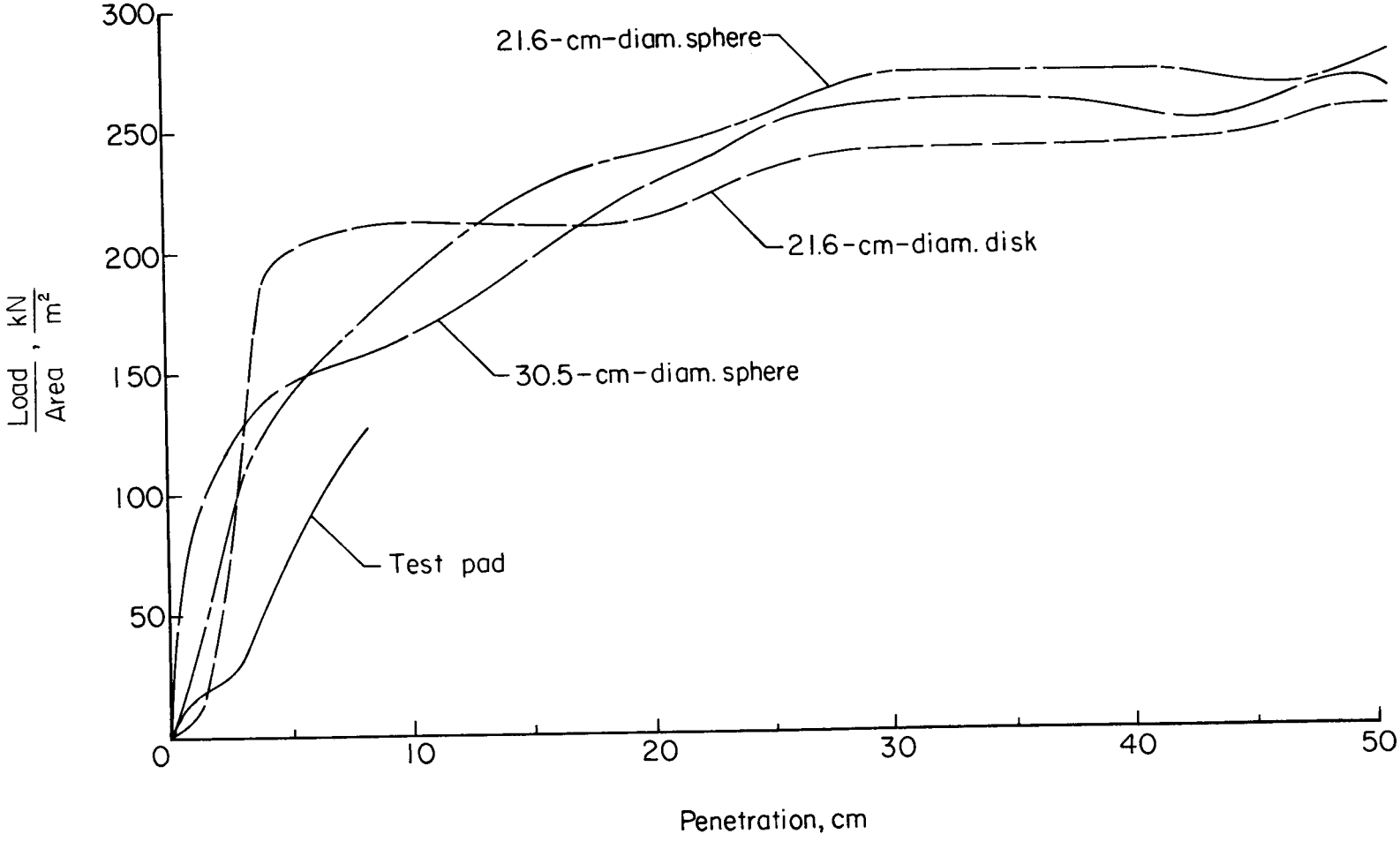

(d) Urethane foam.

Figure 5.- Concluded.

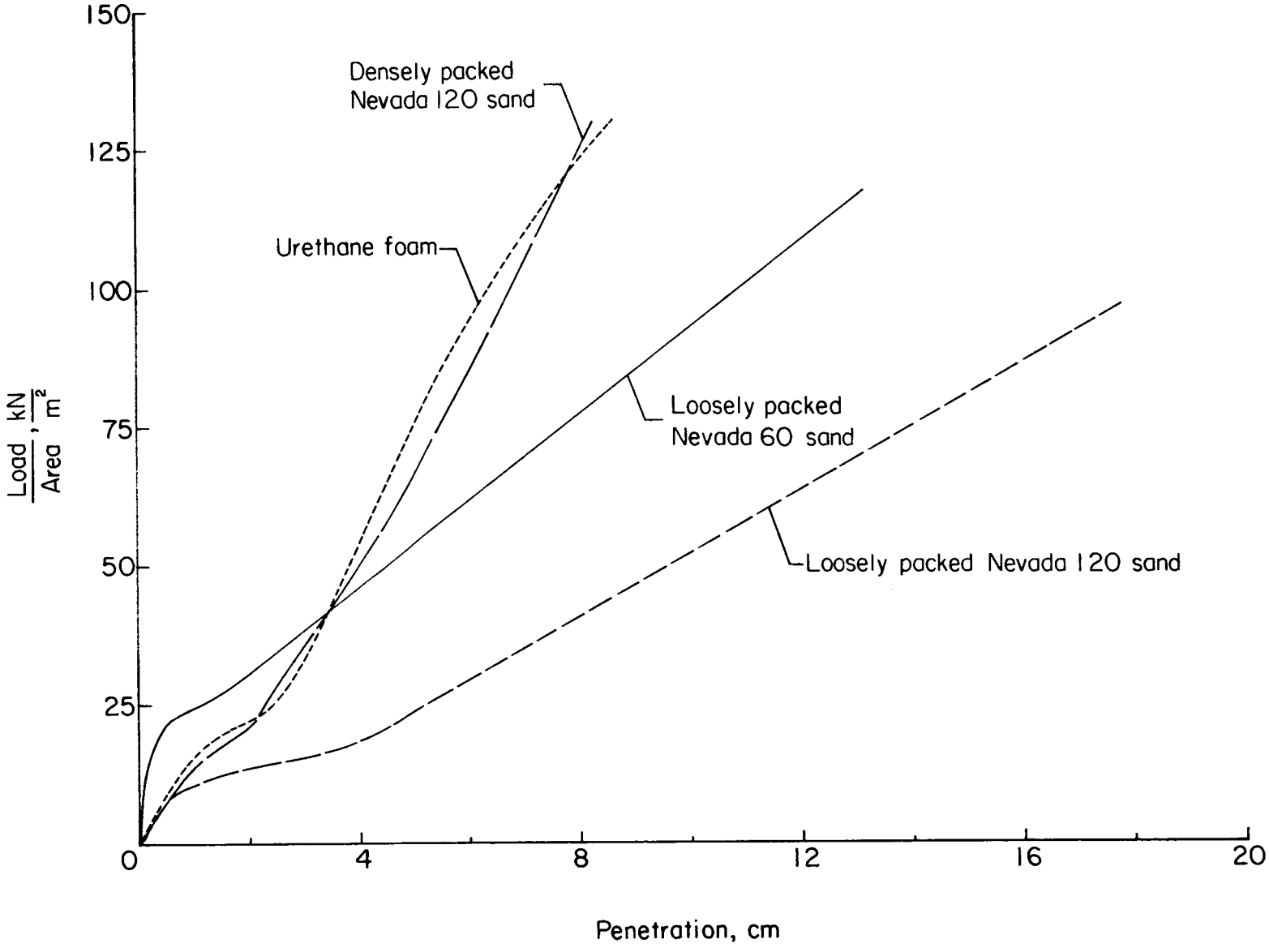

Figure 6.- Summary of results from test pad quasi-static loadings.

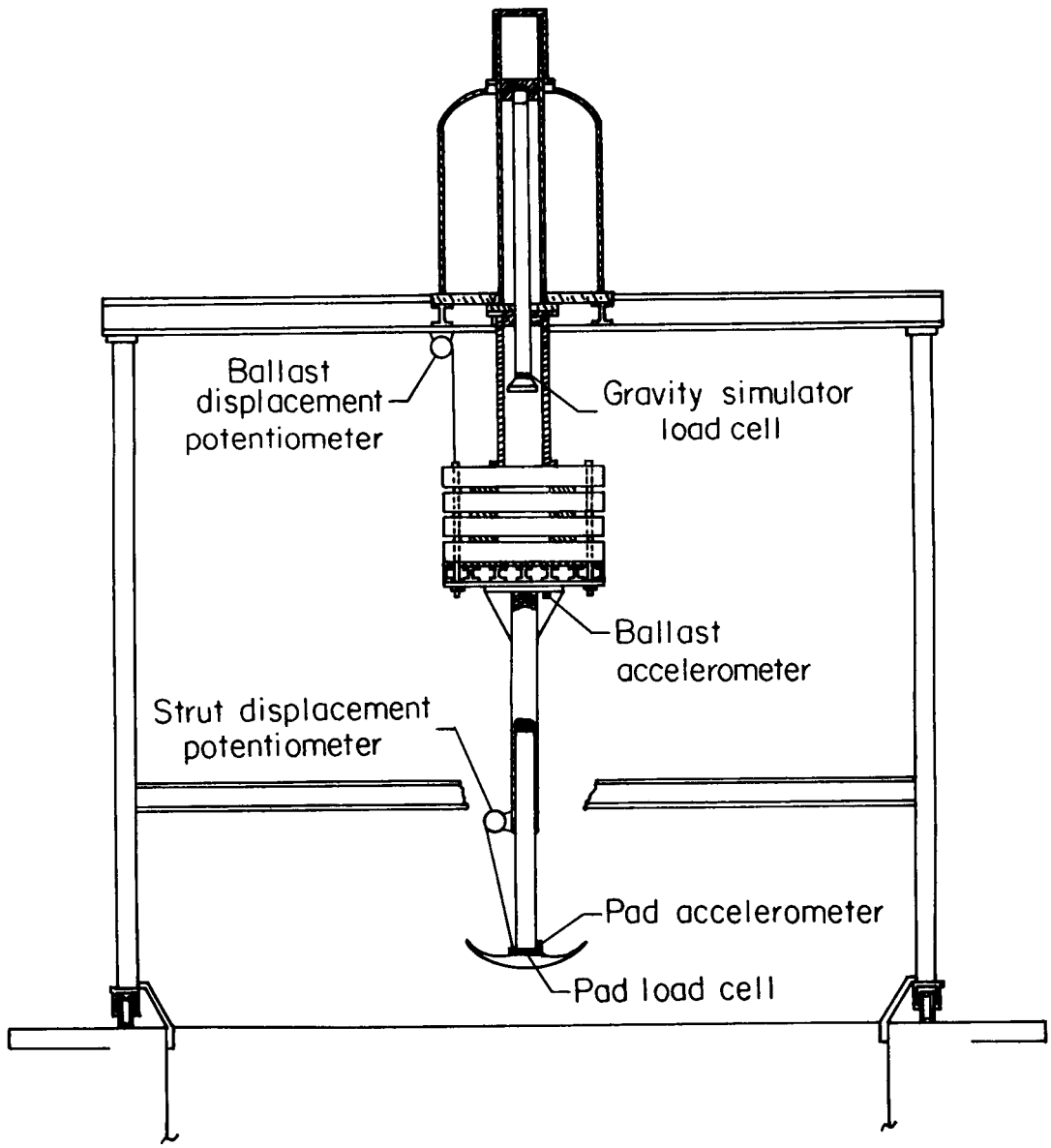

Figure 7.- Test assembly showing location of instrumentation sensors.

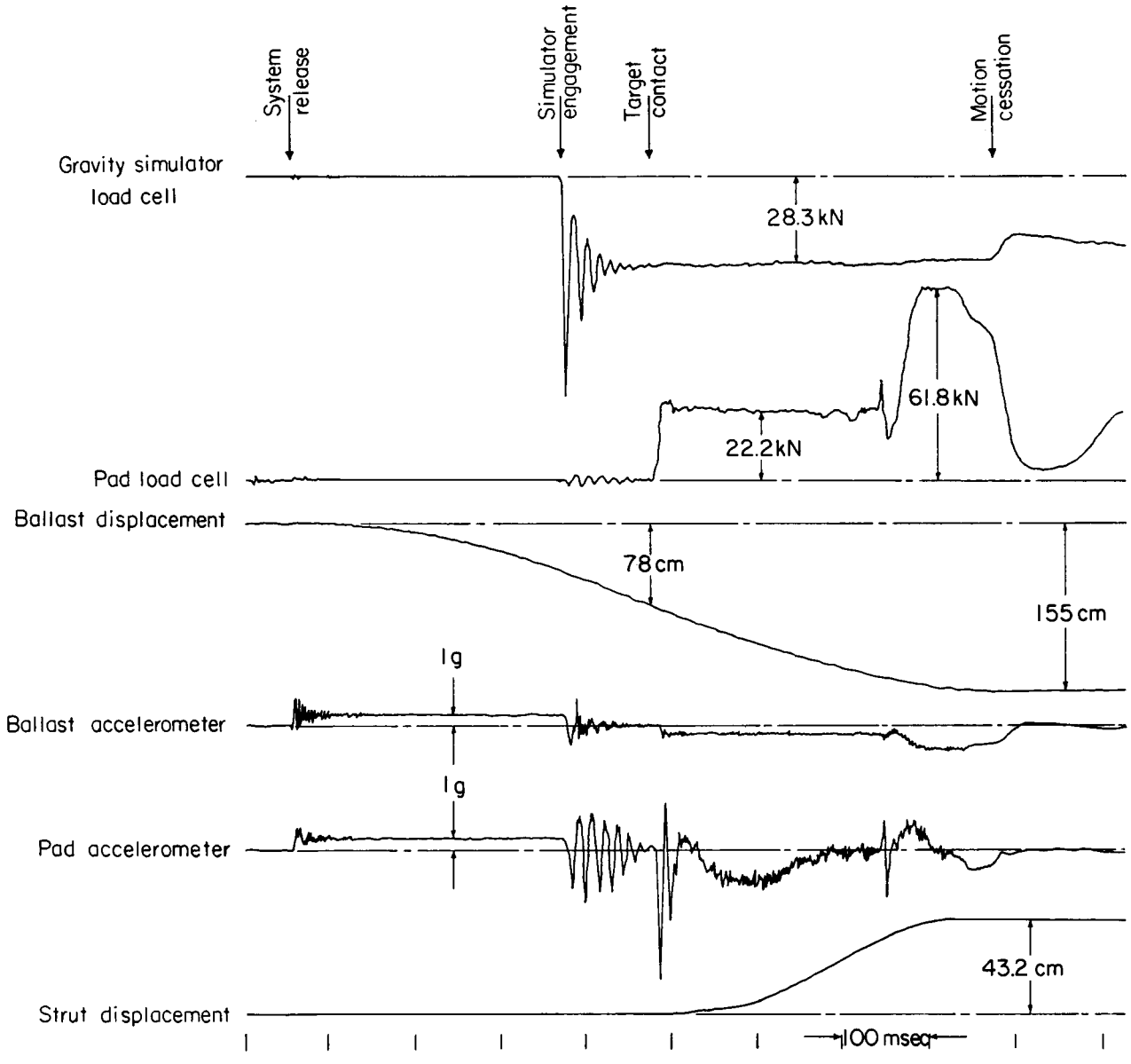

Figure 8.- Reproduction of a typical record of landing gear test. Target, loosely packed Nevada 120 sand; system mass, 3506 kg; impact velocity, 3.02 m/sec.

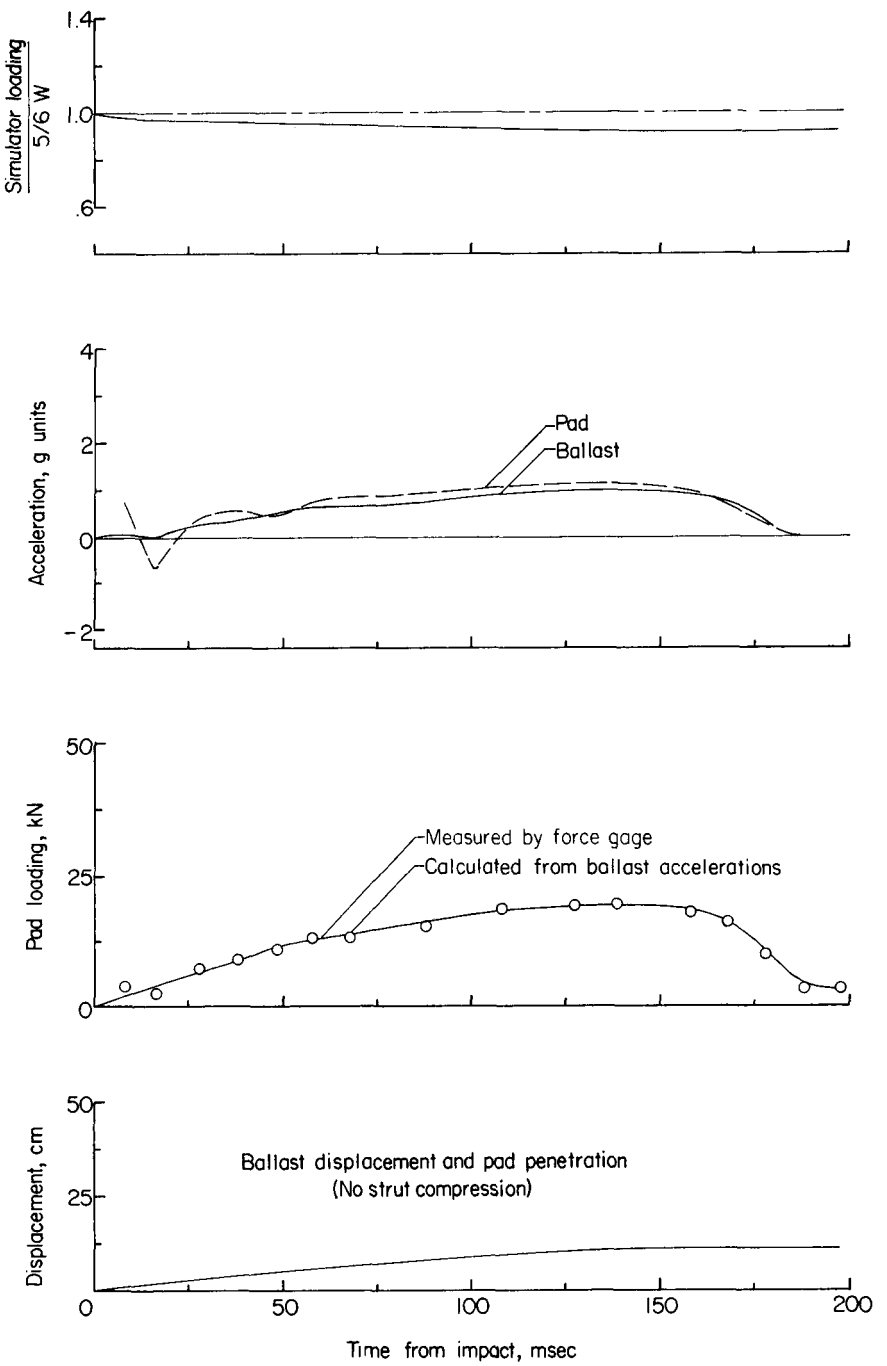

(a) Target, loosely packed Nevada 60 sand; system mass, 1715 kg; impact velocity, 1.08 m/sec.

Figure 9.- Time histories of landing gear response. W is the system earth weight.

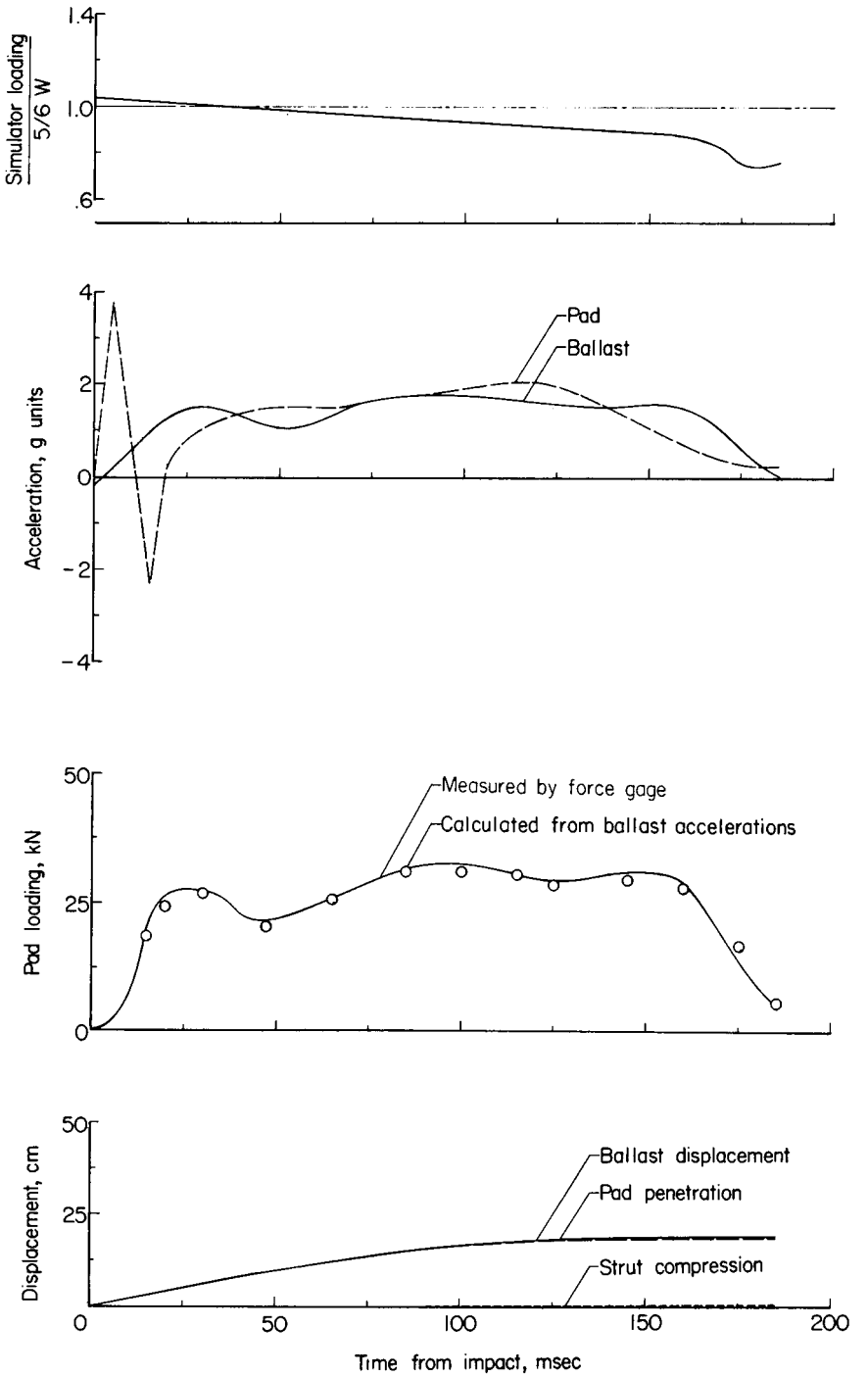

(b) Target, loosely packed Nevada 60 sand; system mass, 1715 kg; impact velocity, 2.22 m/sec.

Figure 9.- Continued.

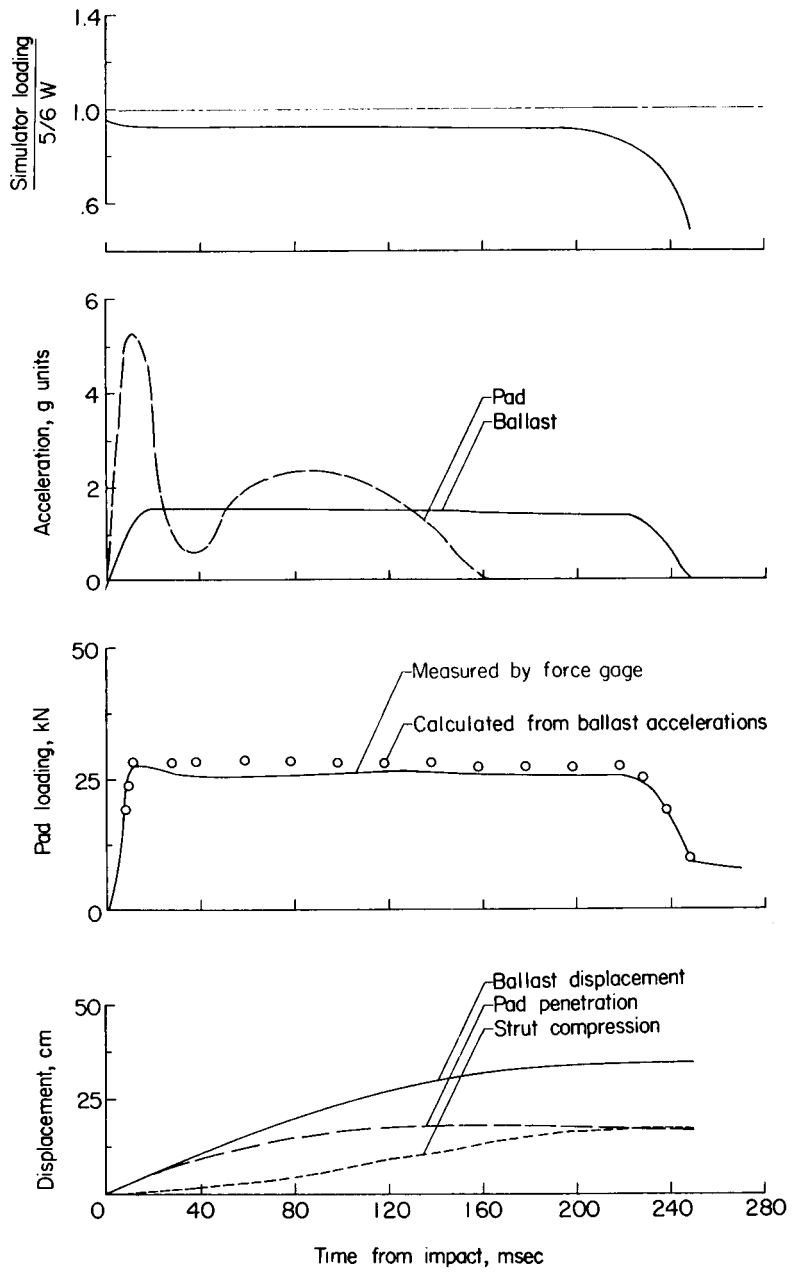

(c) Target, loosely packed Nevada 60 sand; system mass, 1715 kg; impact velocity, 3.02 m/sec.

Figure 9.- Continued.

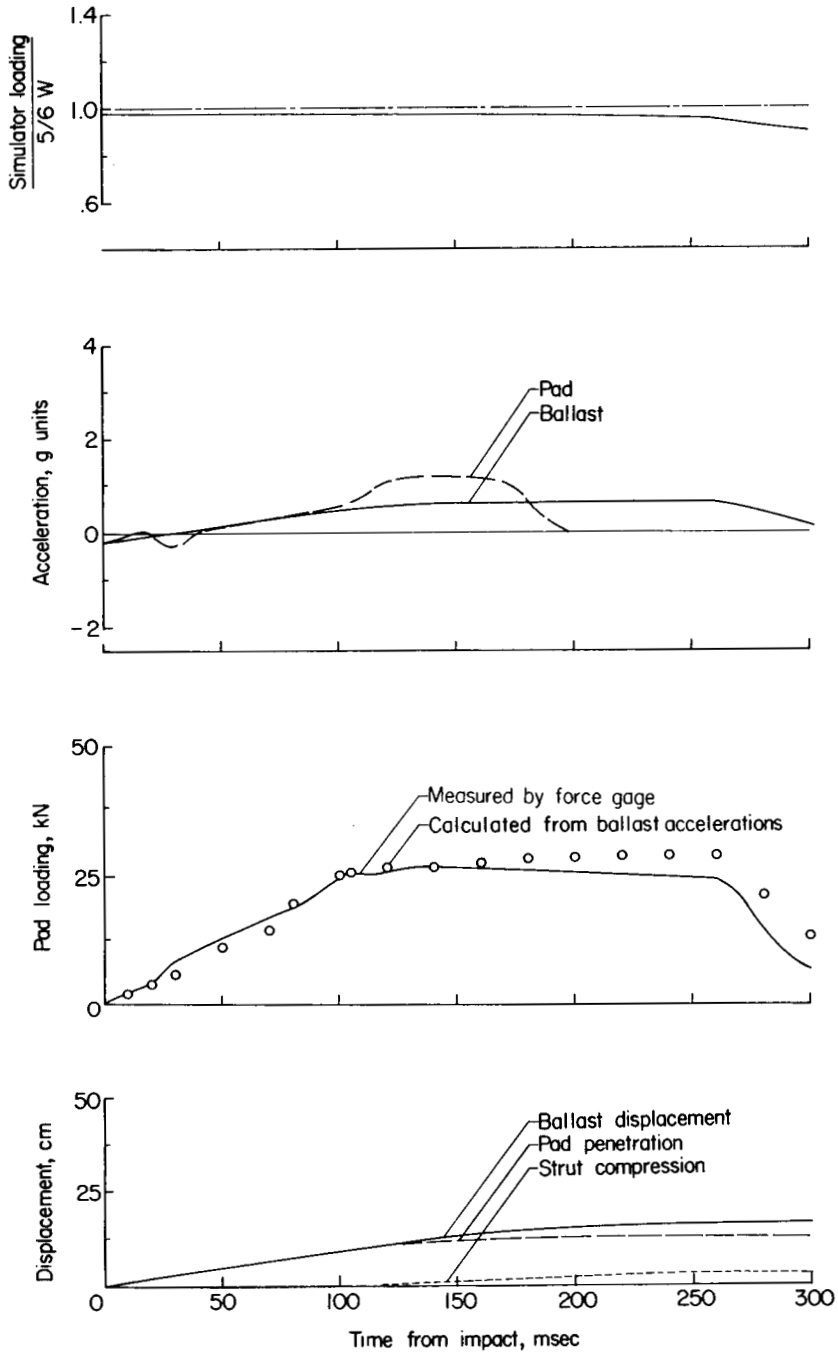

(d) Target, loosely packed Nevada 60 sand; system mass, 3506 kg; impact velocity, 1.10 m/sec.

Figure 9.- Continued.

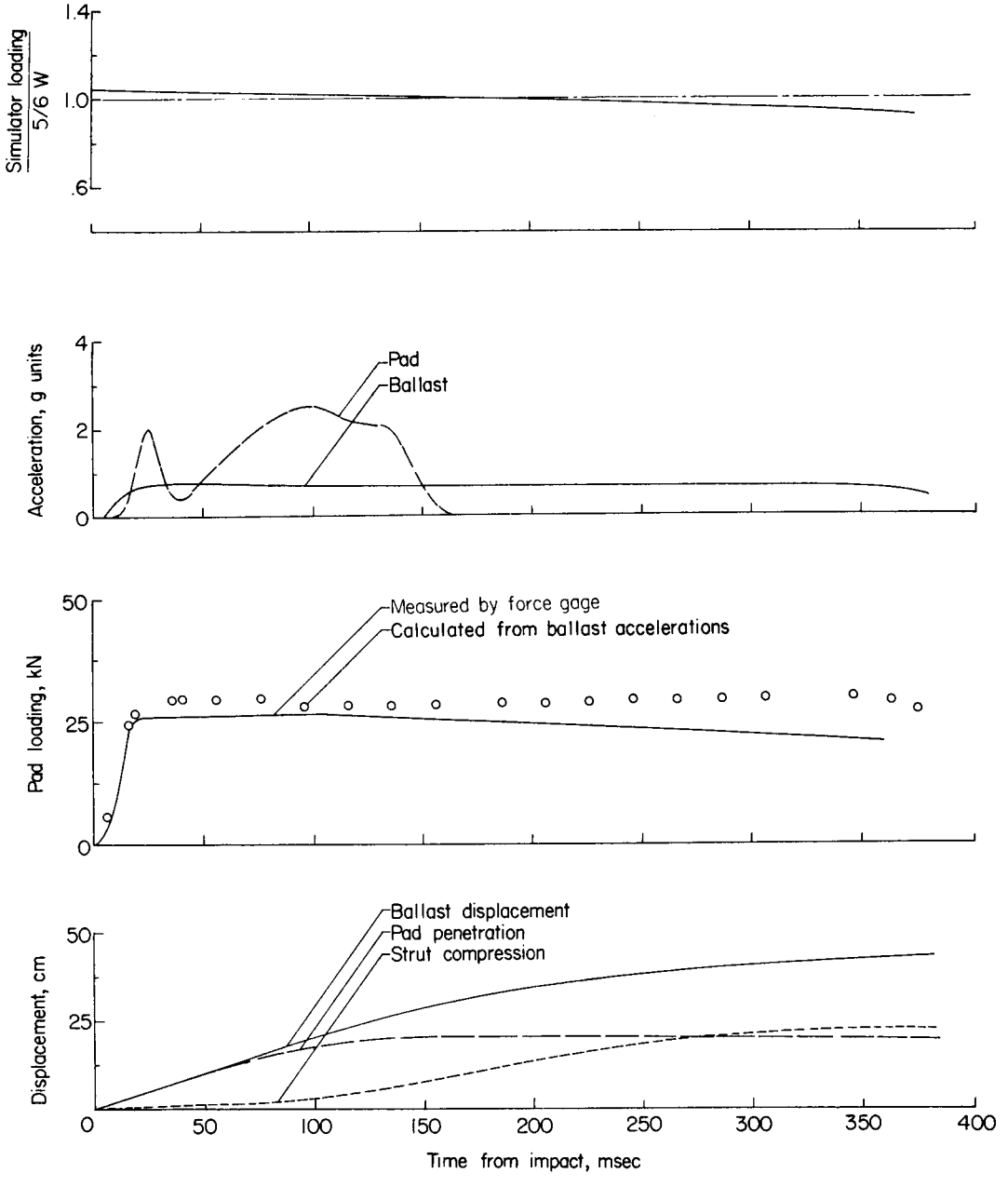

(e) Target, loosely packed Nevada 60 sand; system mass, 3506 kg; impact velocity, 2.32 m/sec.

Figure 9.- Continued.

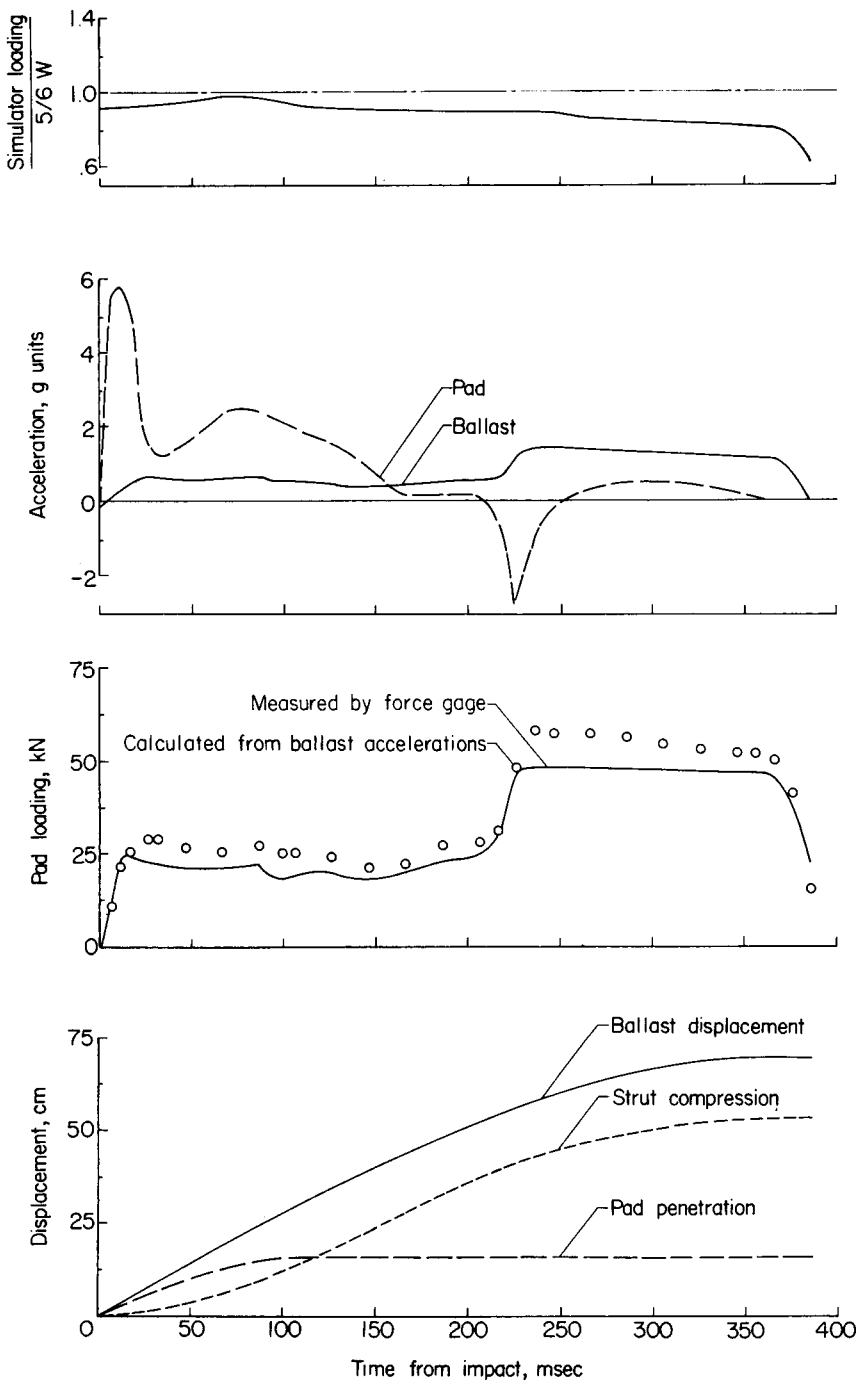

(f) Target, loosely packed Nevada 60 sand; system mass, 3506 kg; impact velocity, 2.99 m/sec.

Figure 9.- Continued.

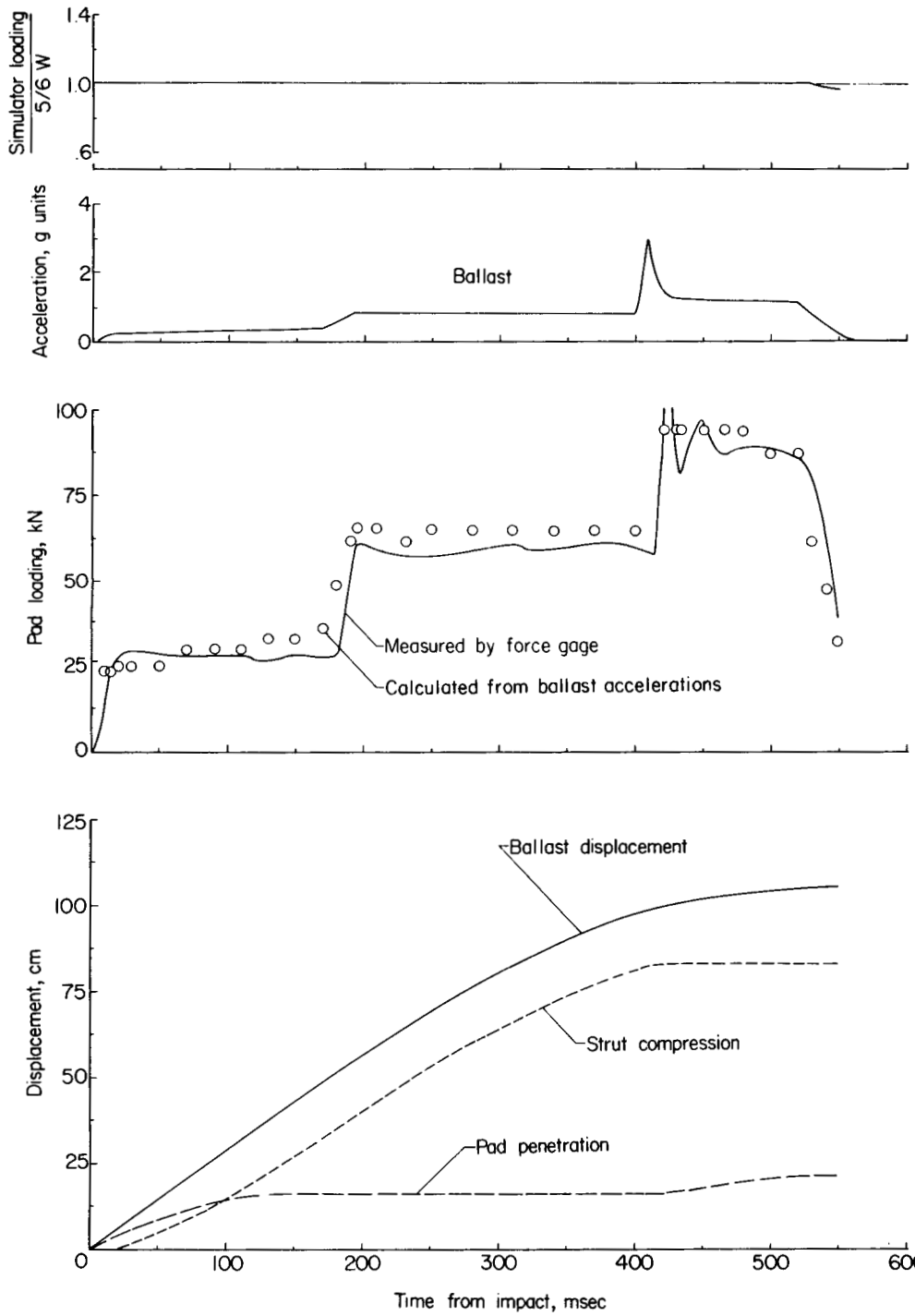

(g) Target, loosely packed Nevada 60 sand; system mass, 6845 kg; impact velocity, 3.05 m/sec.

Figure 9.- Continued.

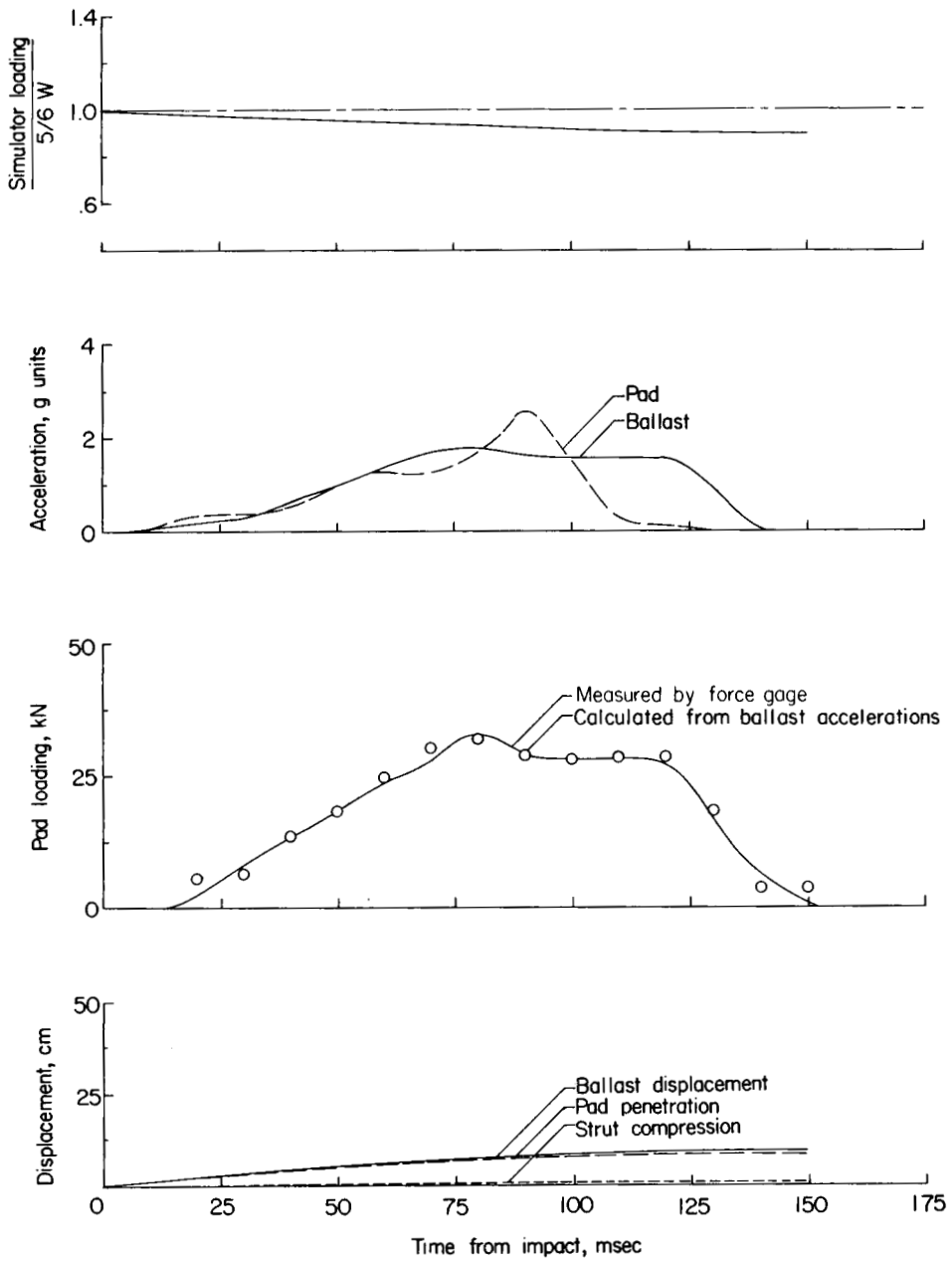

(h) Target, densely packed Nevada 120 sand; system mass, 1715 kg; impact velocity, 1.16 m/sec.

Figure 9.- Continued.

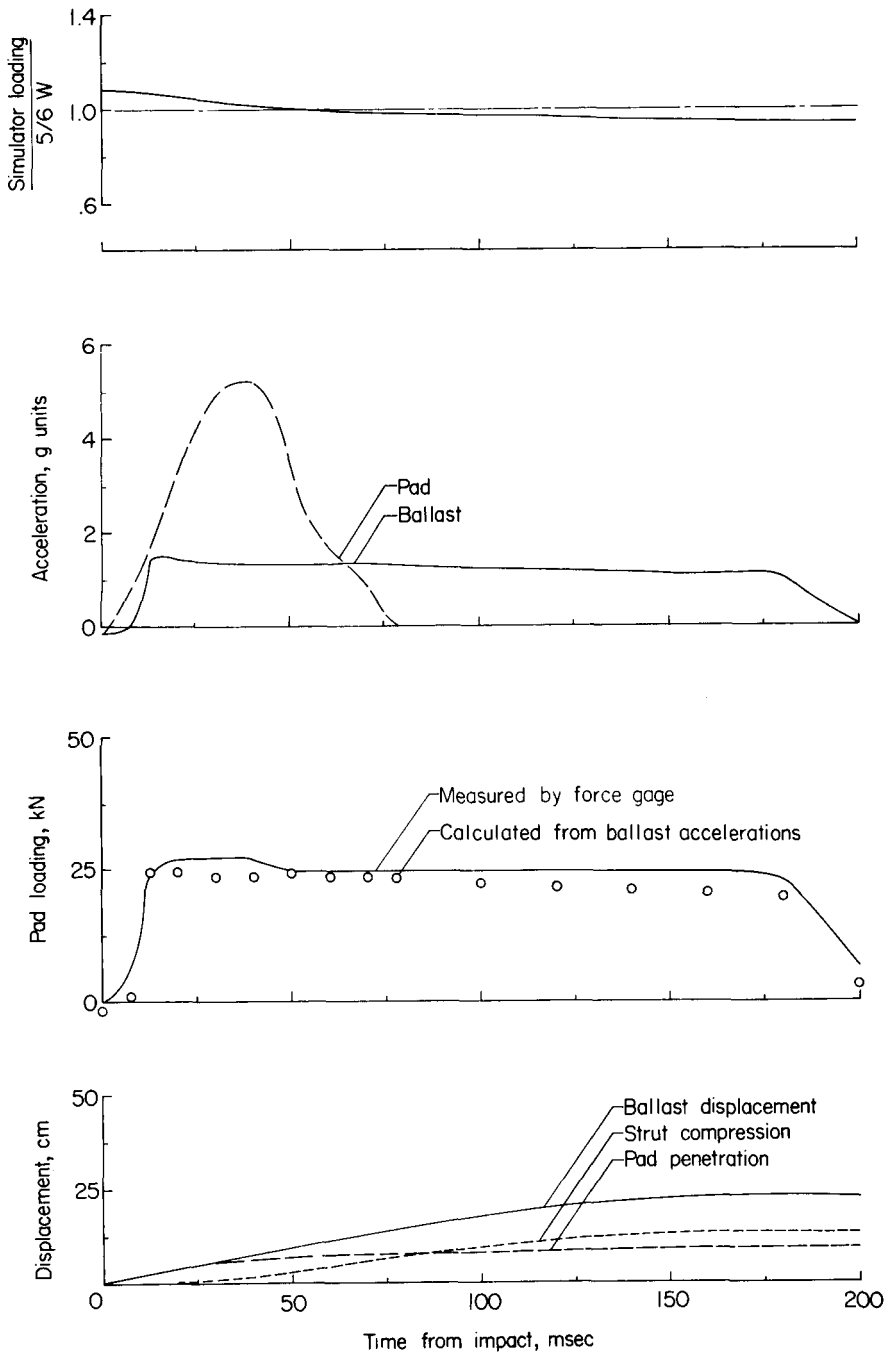

(i) Target, densely packed Nevada 120 sand; system mass, 1715 kg; impact velocity, 2.24 m/sec.

Figure 9.- Continued.

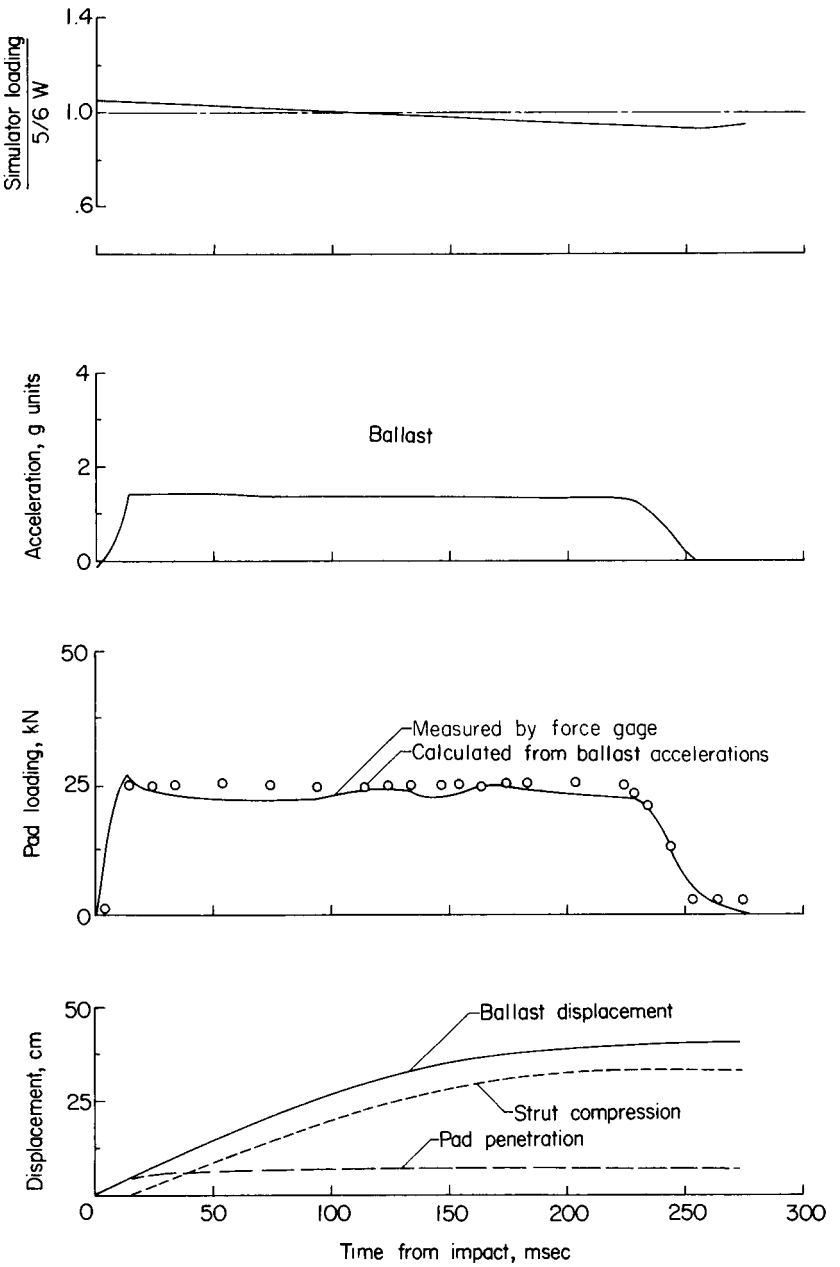

(j) Target, densely packed Nevada 120 sand; system mass, 1715 kg; impact velocity, 3.05 m/sec.

Figure 9.- Continued.

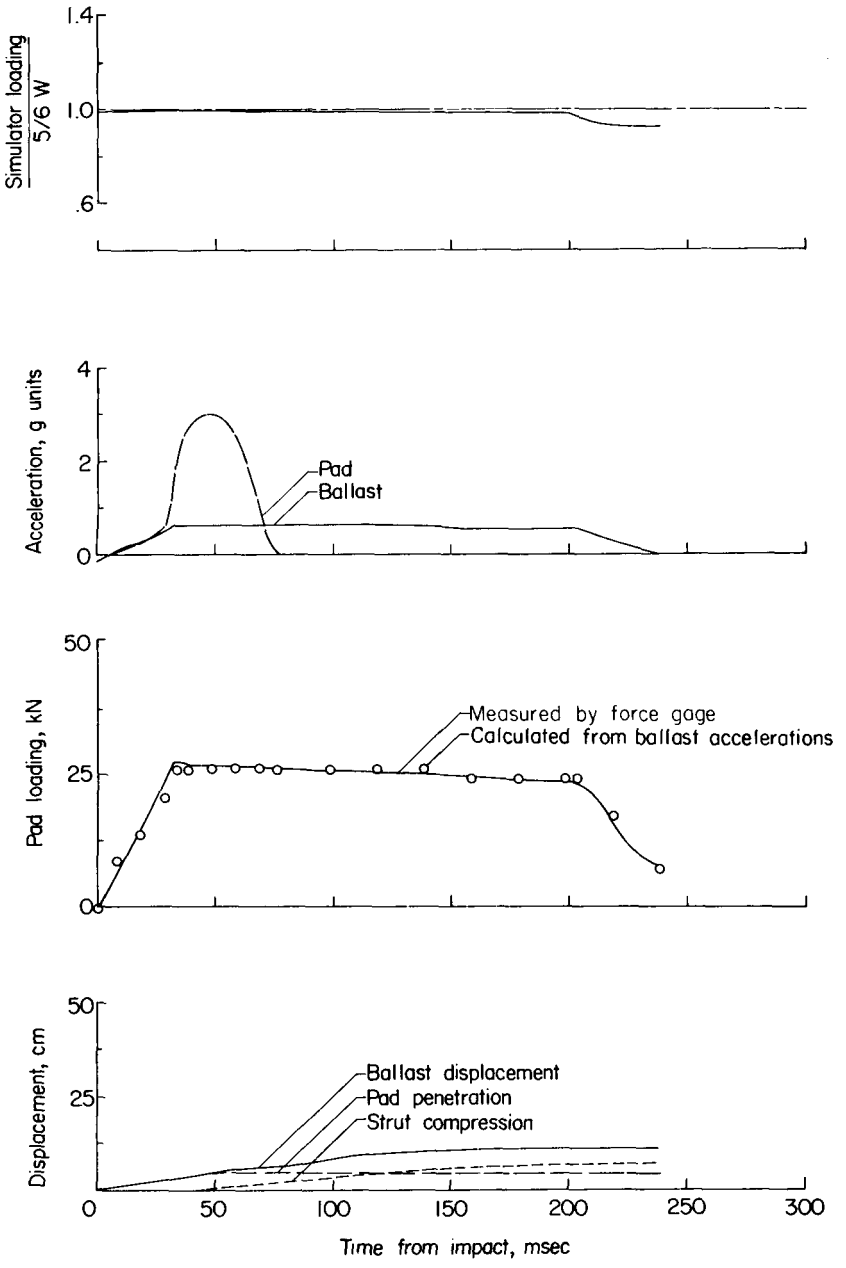

(k) Target, densely packed Nevada 120 sand; system mass, 3506 kg; impact velocity, 1.16 m/sec.

Figure 9.- Continued.

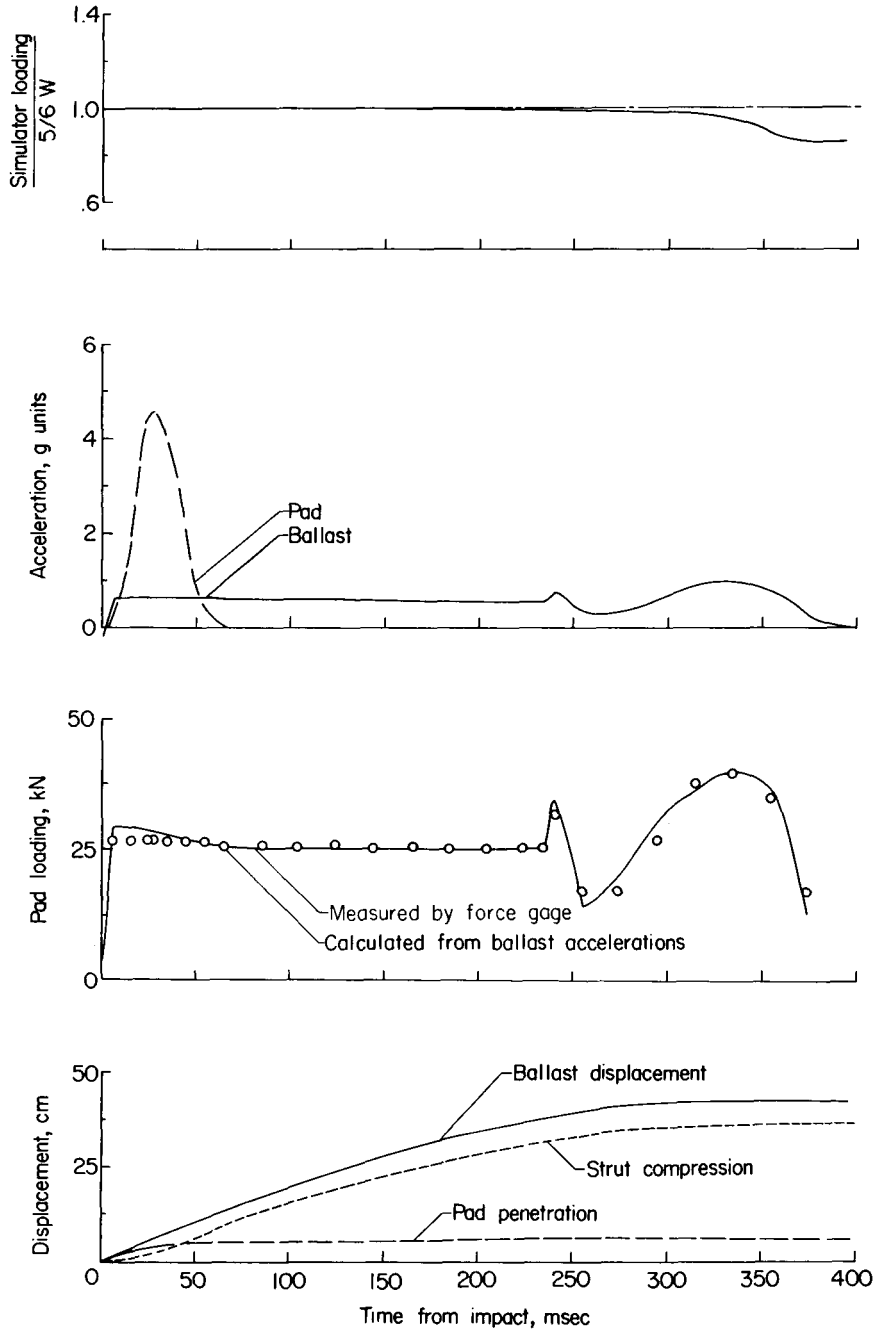

(l) Target, densely packed Nevada 120 sand; system mass, 3506 kg; impact velocity, 2.41 m/sec.

Figure 9.- Continued.

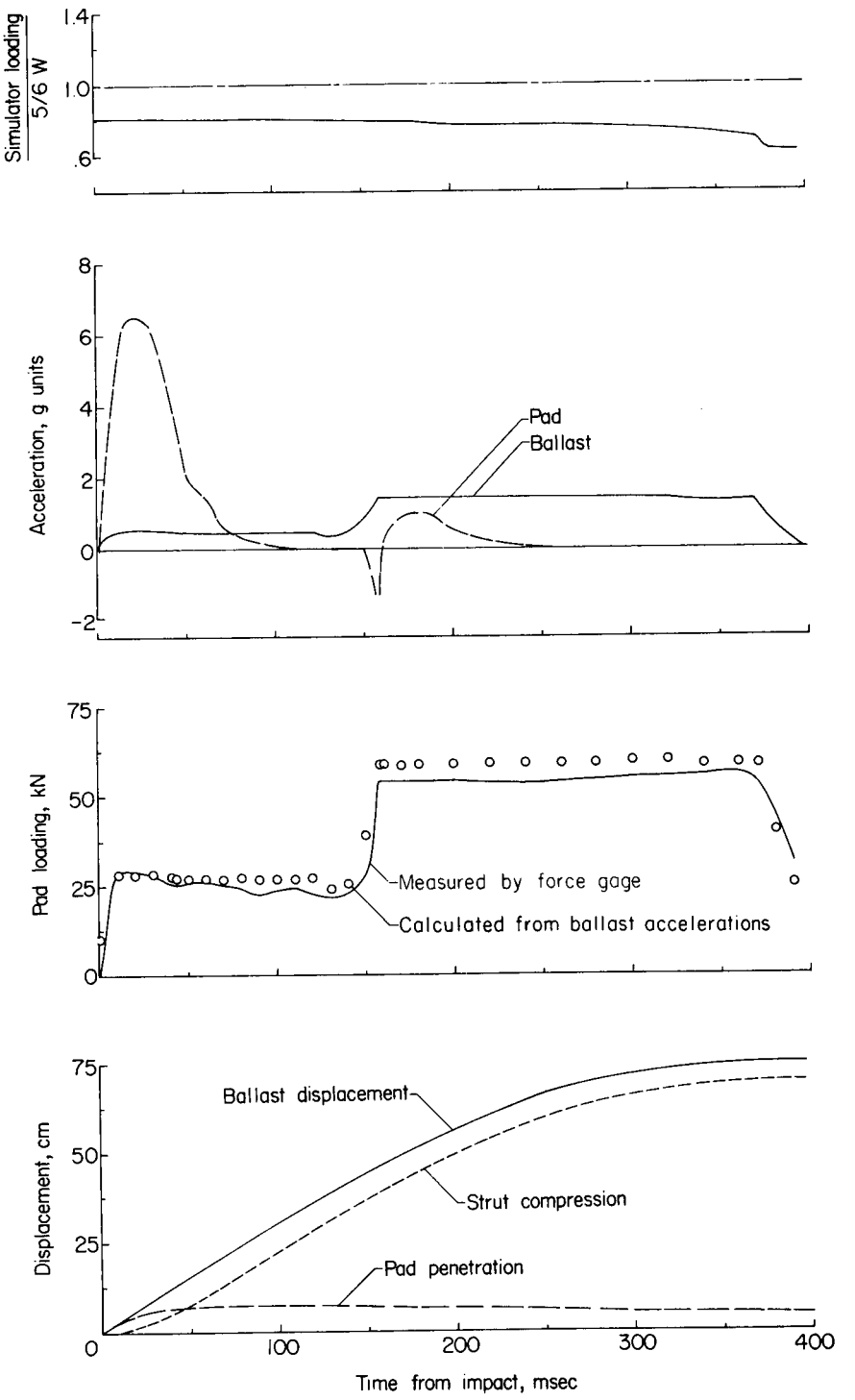

(m) Target, densely packed Nevada 120 sand; system mass, 3506 kg; impact velocity, 3.20 m/sec.

Figure 9.- Continued.

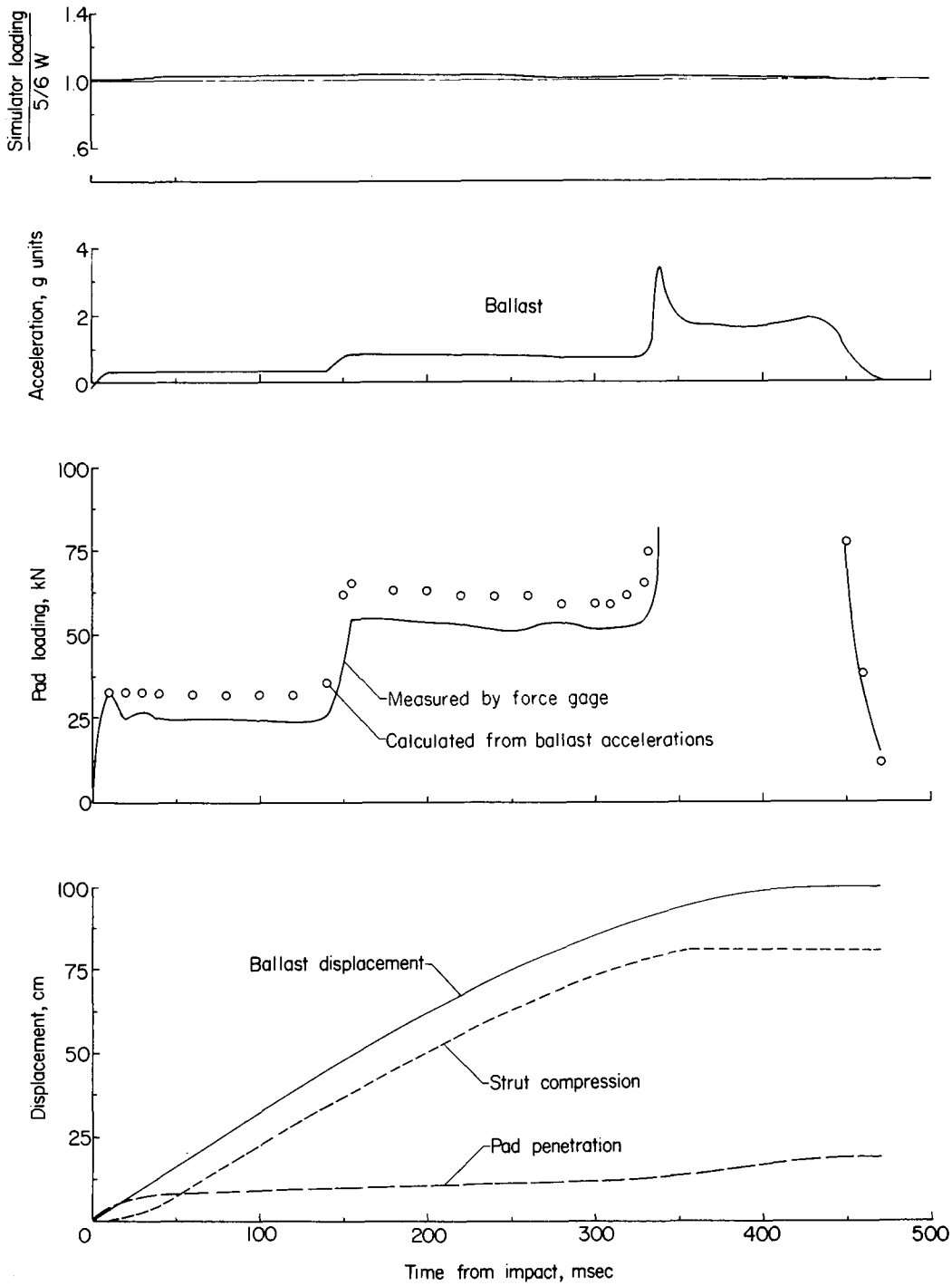

(n) Target, densely packed Nevada 120 sand; system mass, 6845 kg; impact velocity, 3.11 m/sec.

Figure 9.- Continued.

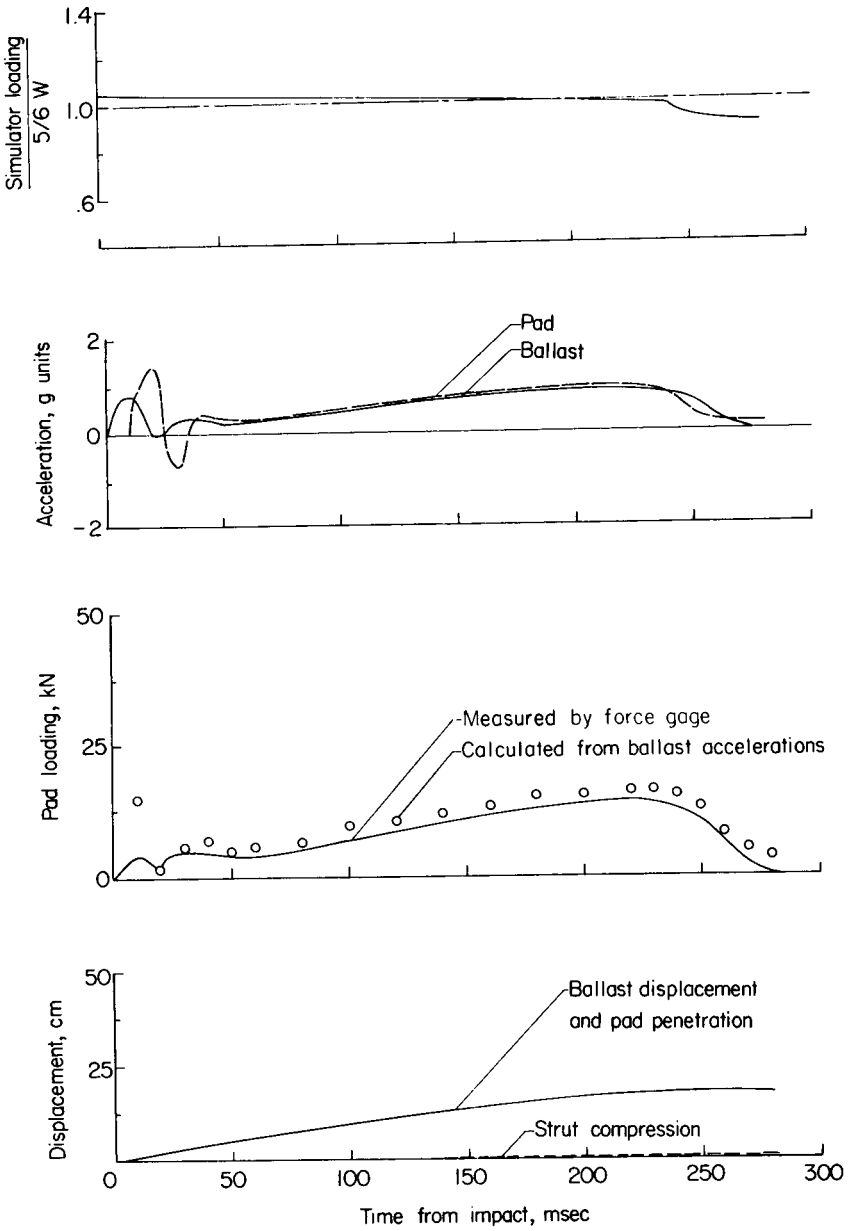

(o) Target, loosely packed Nevada 120 sand; system mass, 1715 kg; impact velocity, 1.06 m/sec.

Figure 9.- Continued.

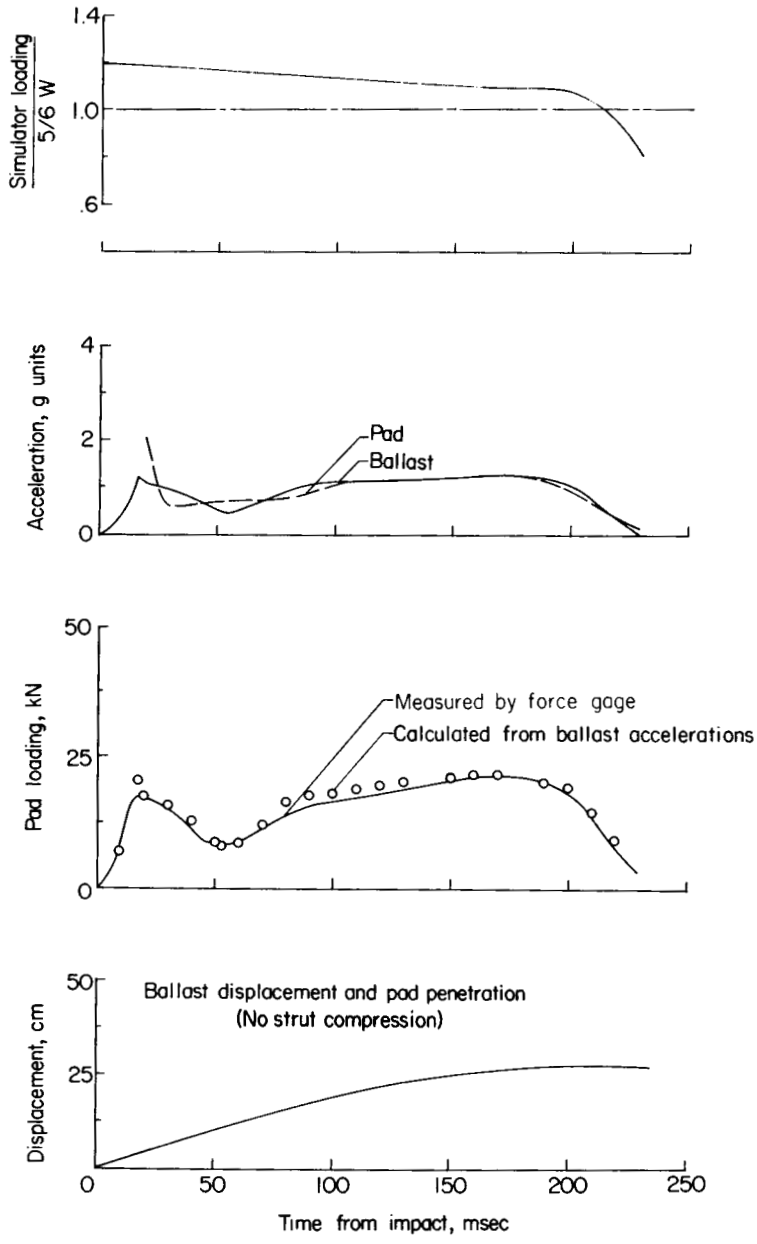

(p) Target, loosely packed Nevada 120 sand; system mass, 1715 kg; impact velocity, 2.21 m/sec.

Figure 9.- Continued.

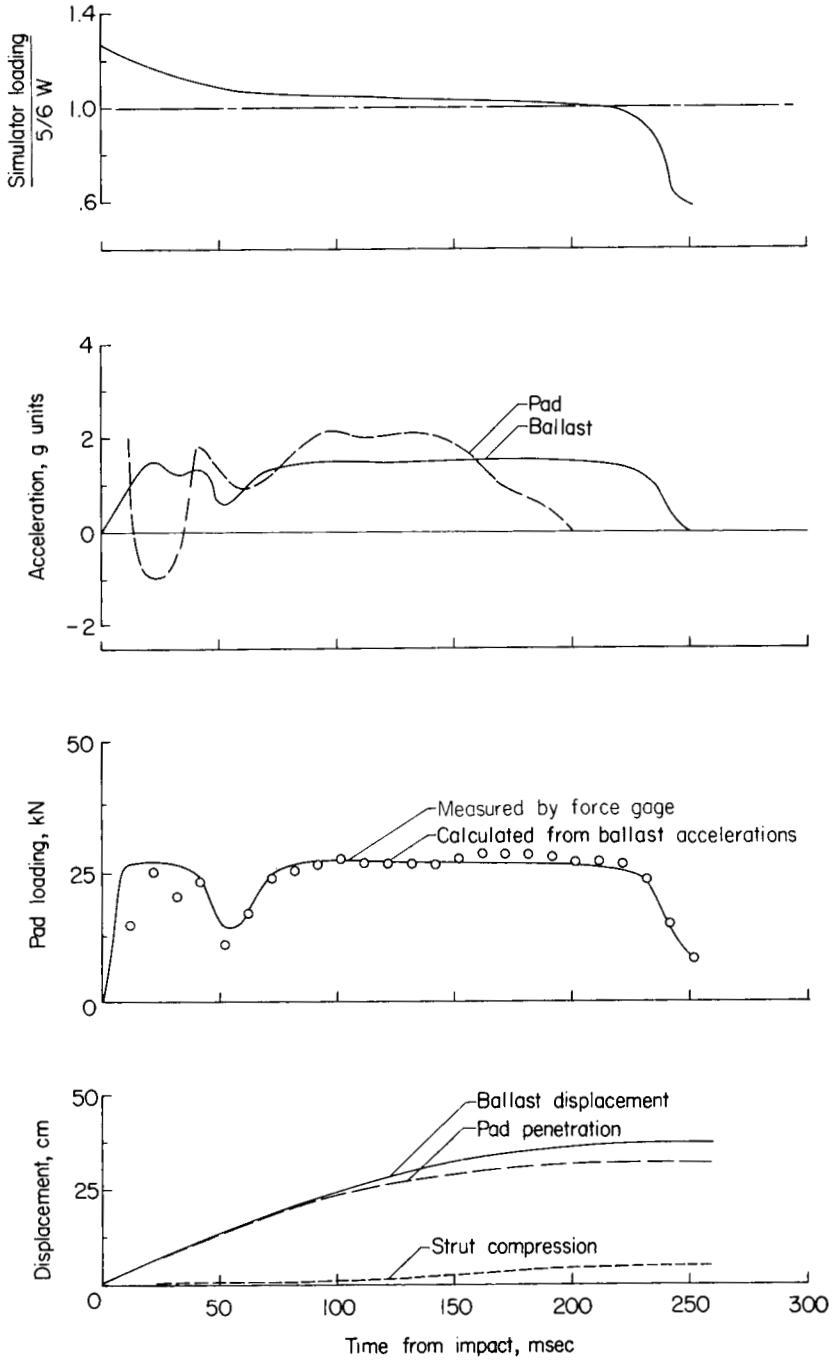

(q) Target, loosely packed Nevada 120 sand; system mass, 1715 kg; impact velocity, 2.99 m/sec.

Figure 9.- Continued.

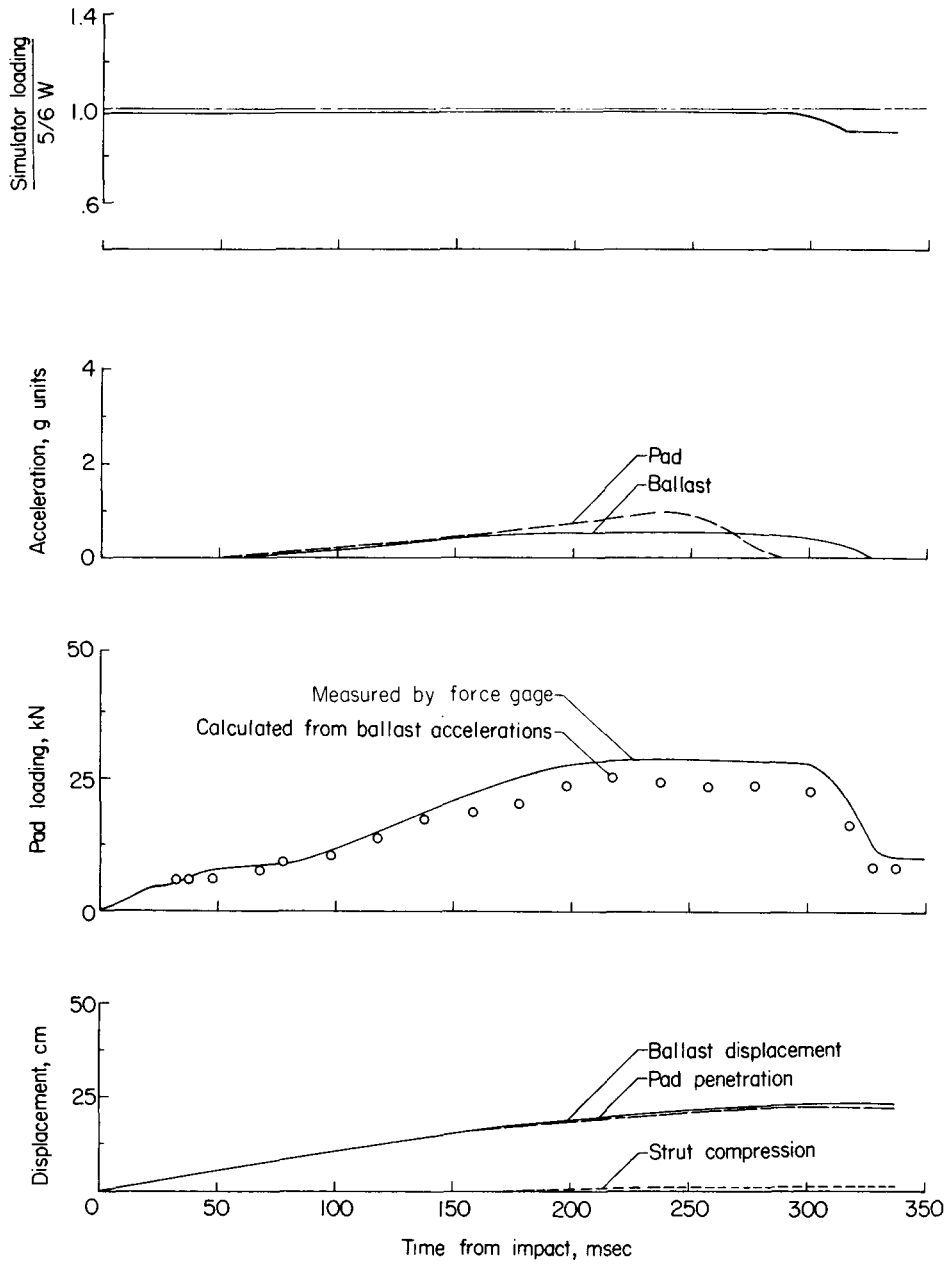

(r) Target, loosely packed Nevada 120 sand; system mass, 3506 kg; impact velocity, 0.99 m/sec.

Figure 9.- Continued.

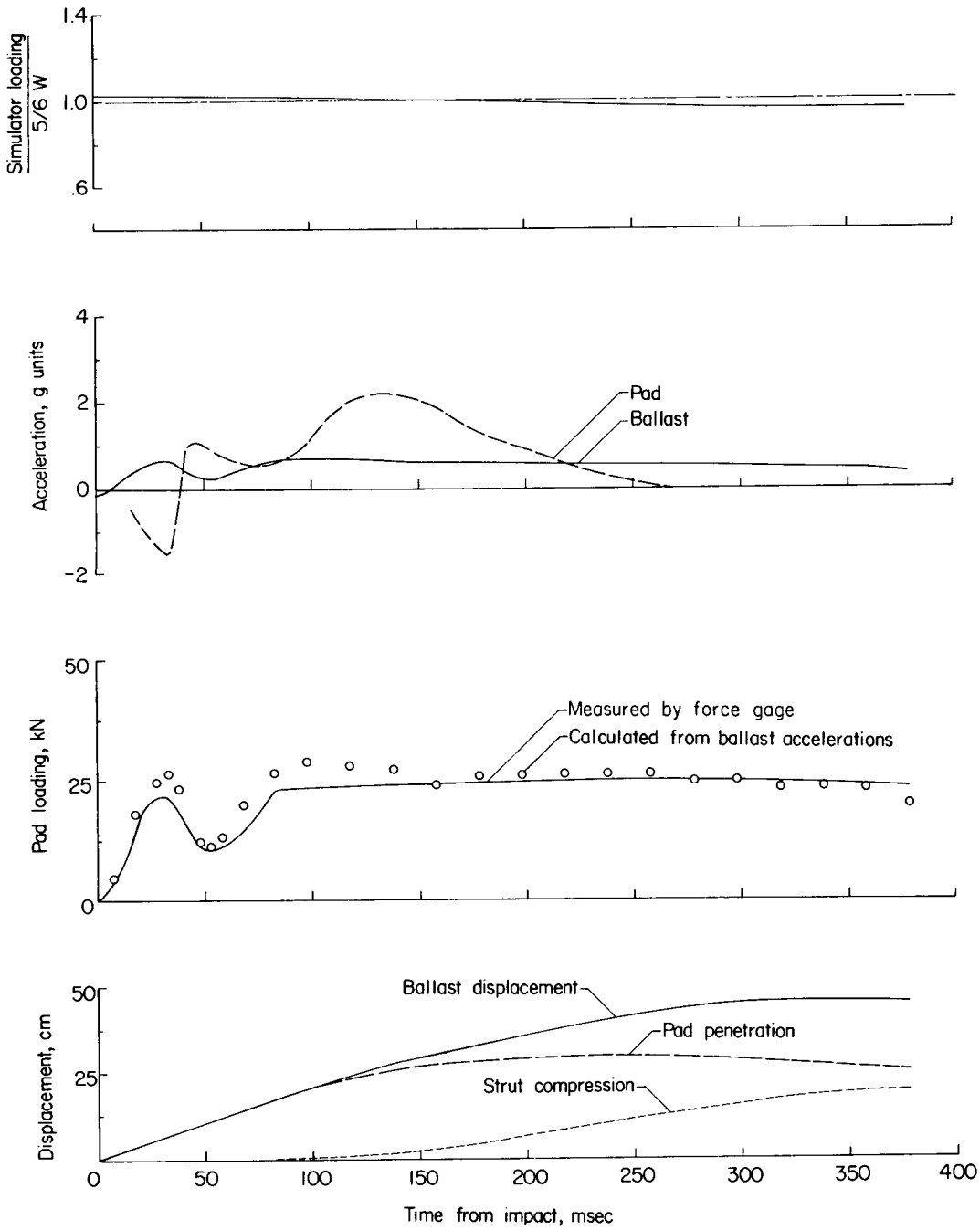

(s) Target, loosely packed Nevada 120 sand; system mass, 3506 kg; impact velocity, 2.35 m/sec.

Figure 9.- Continued.

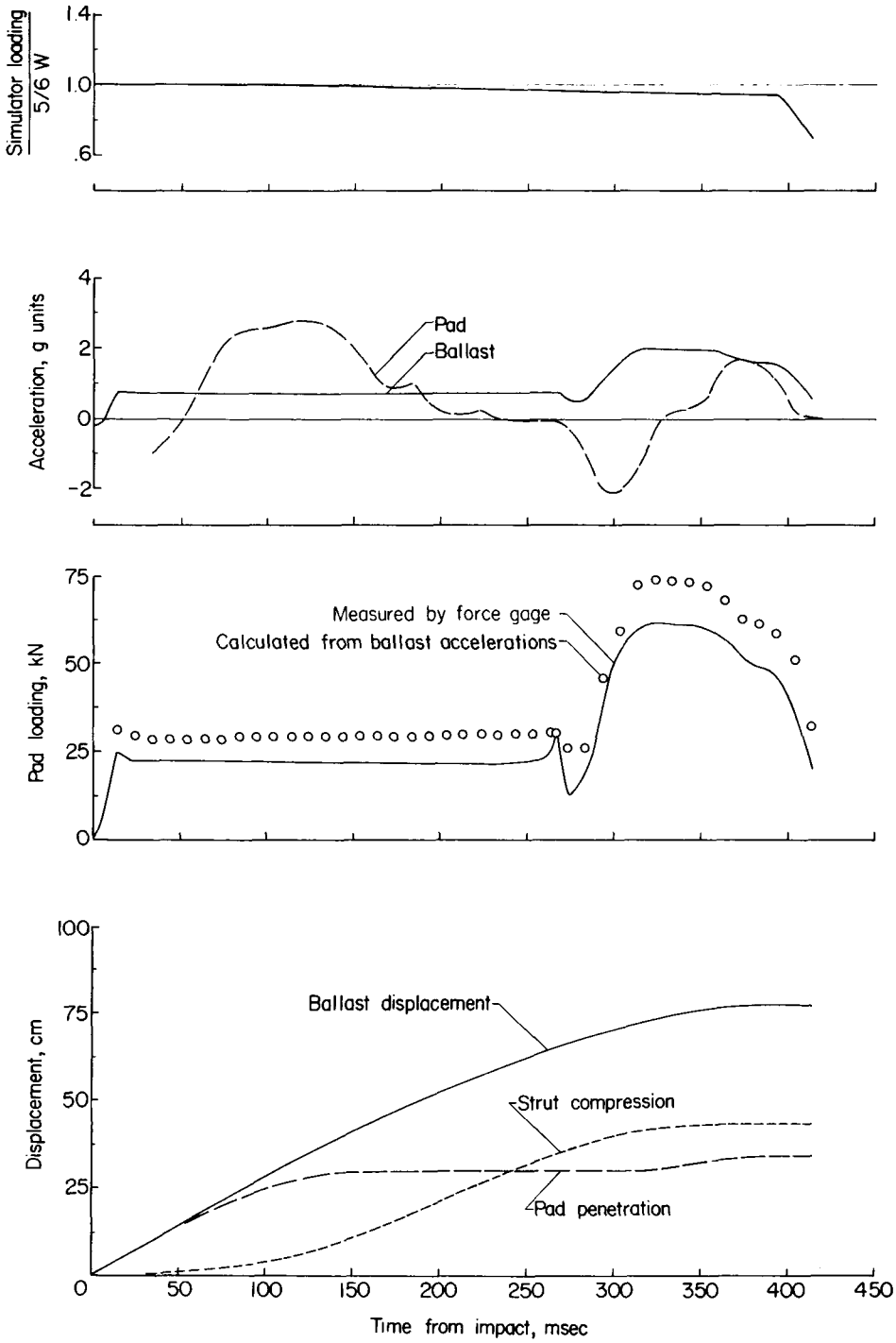

(t) Target, loosely packed Nevada 120 sand; system mass, 3506 kg; impact velocity, 3.02 m/sec.

Figure 9.- Continued.

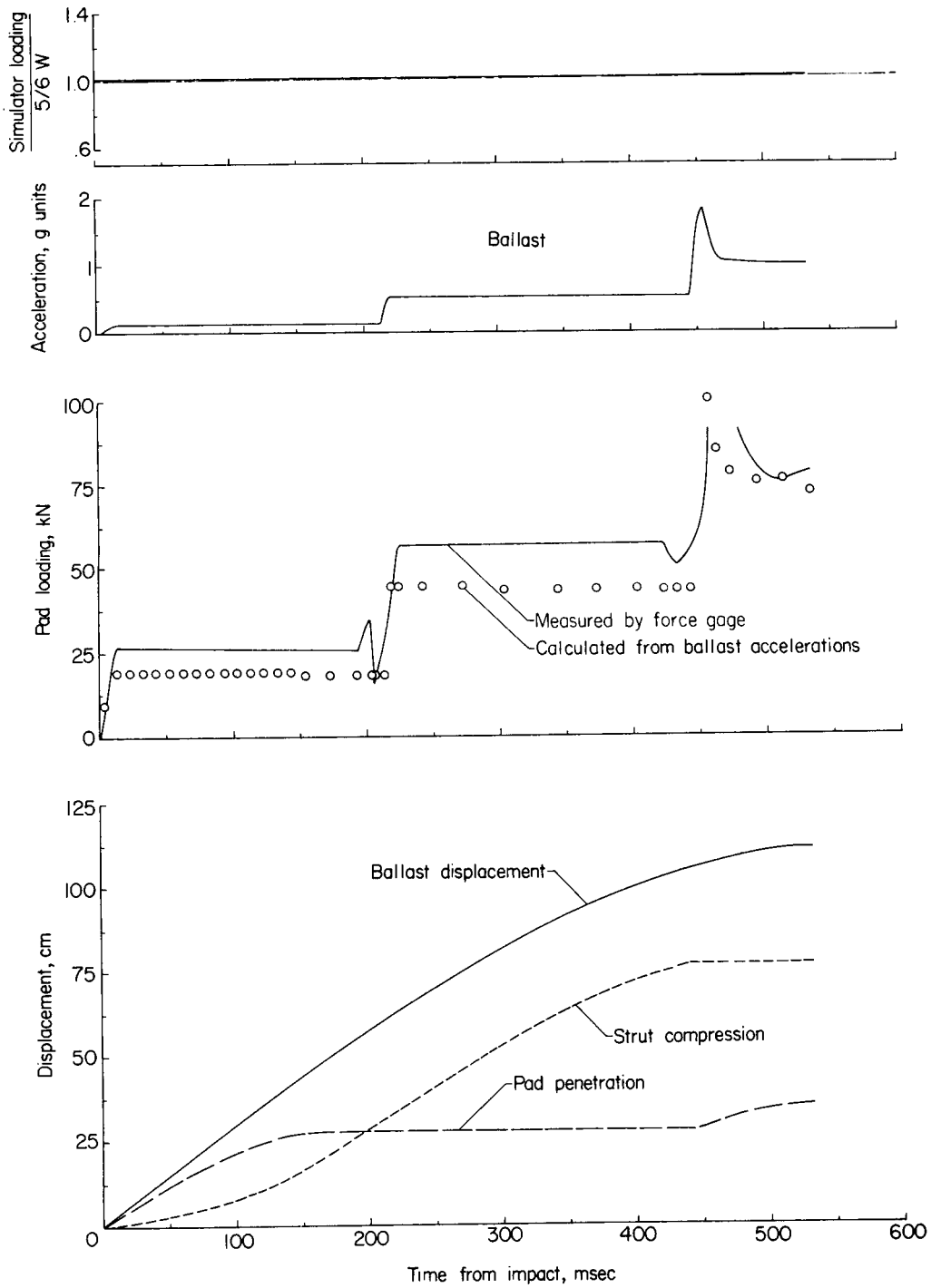

(u) Target, loosely packed Nevada 120 sand; system mass, 6845 kg; impact velocity, 3.05 m/sec.

Figure 9.- Continued.

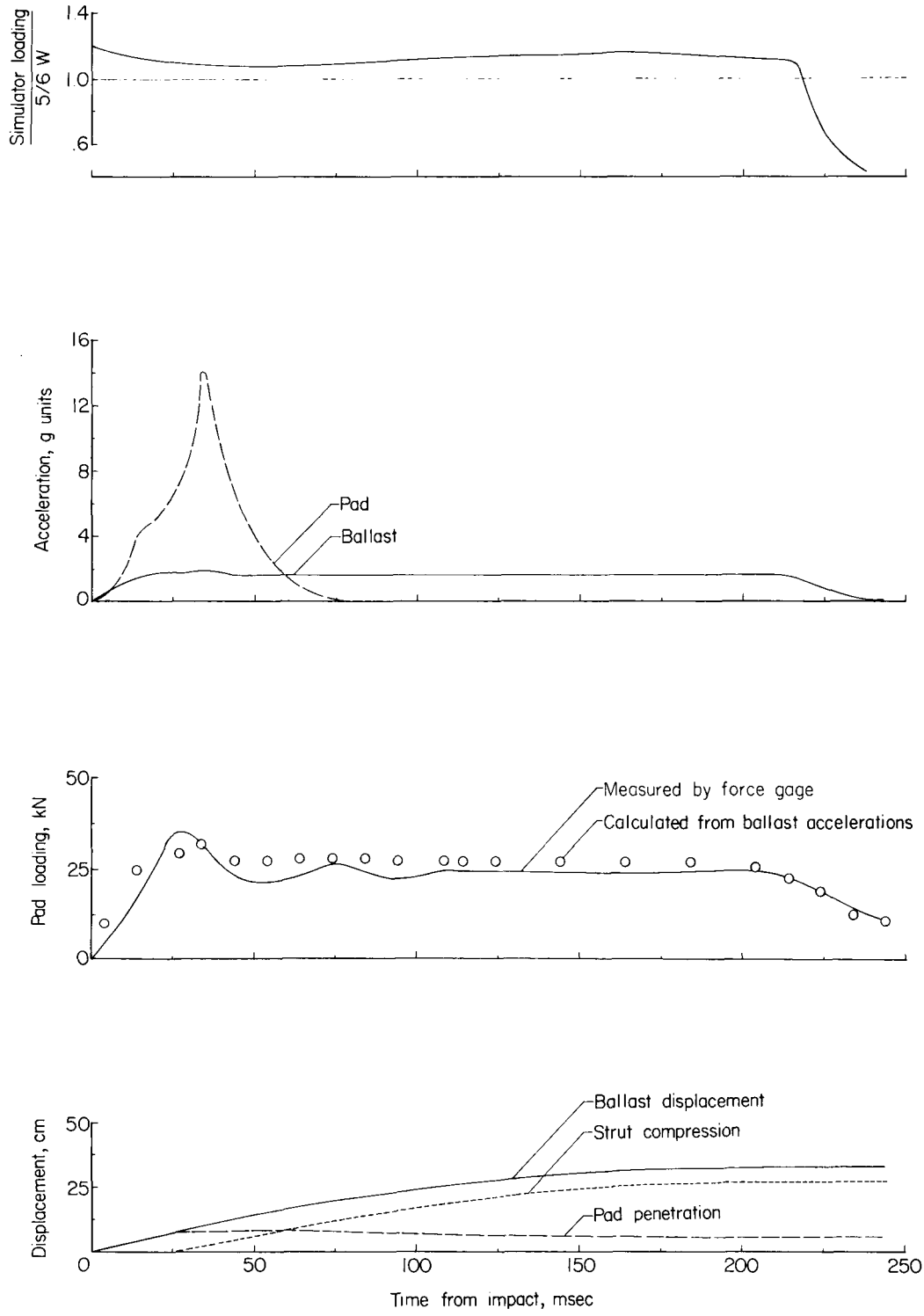

(v) Target, urethane foam; system mass, 1715 kg; impact velocity, 3.05 m/sec.

Figure 9.- Continued.

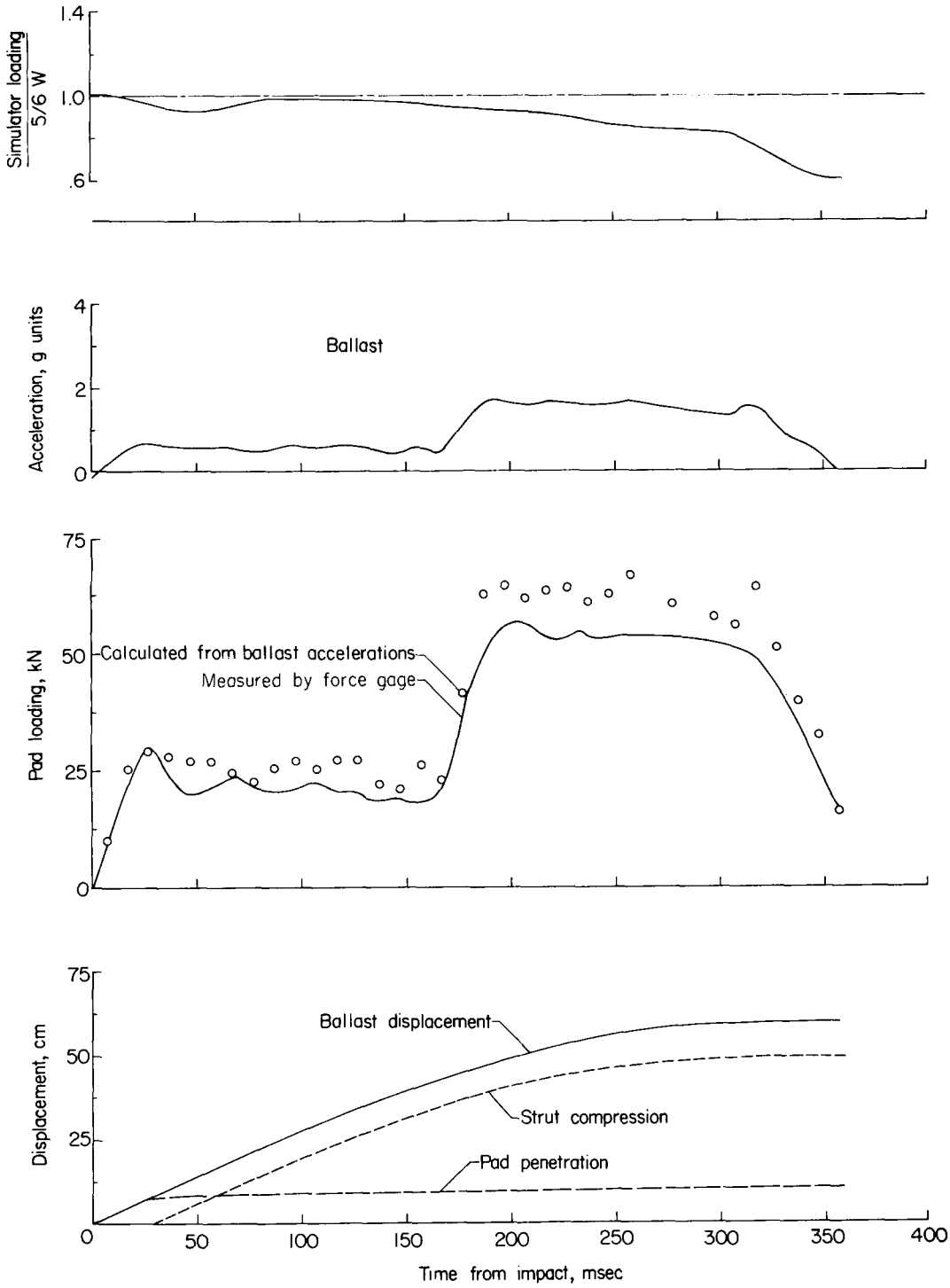

(w) Target, urethane foam; system mass, 3506 kg; impact velocity, 3.05 m/sec.

Figure 9.- Continued.

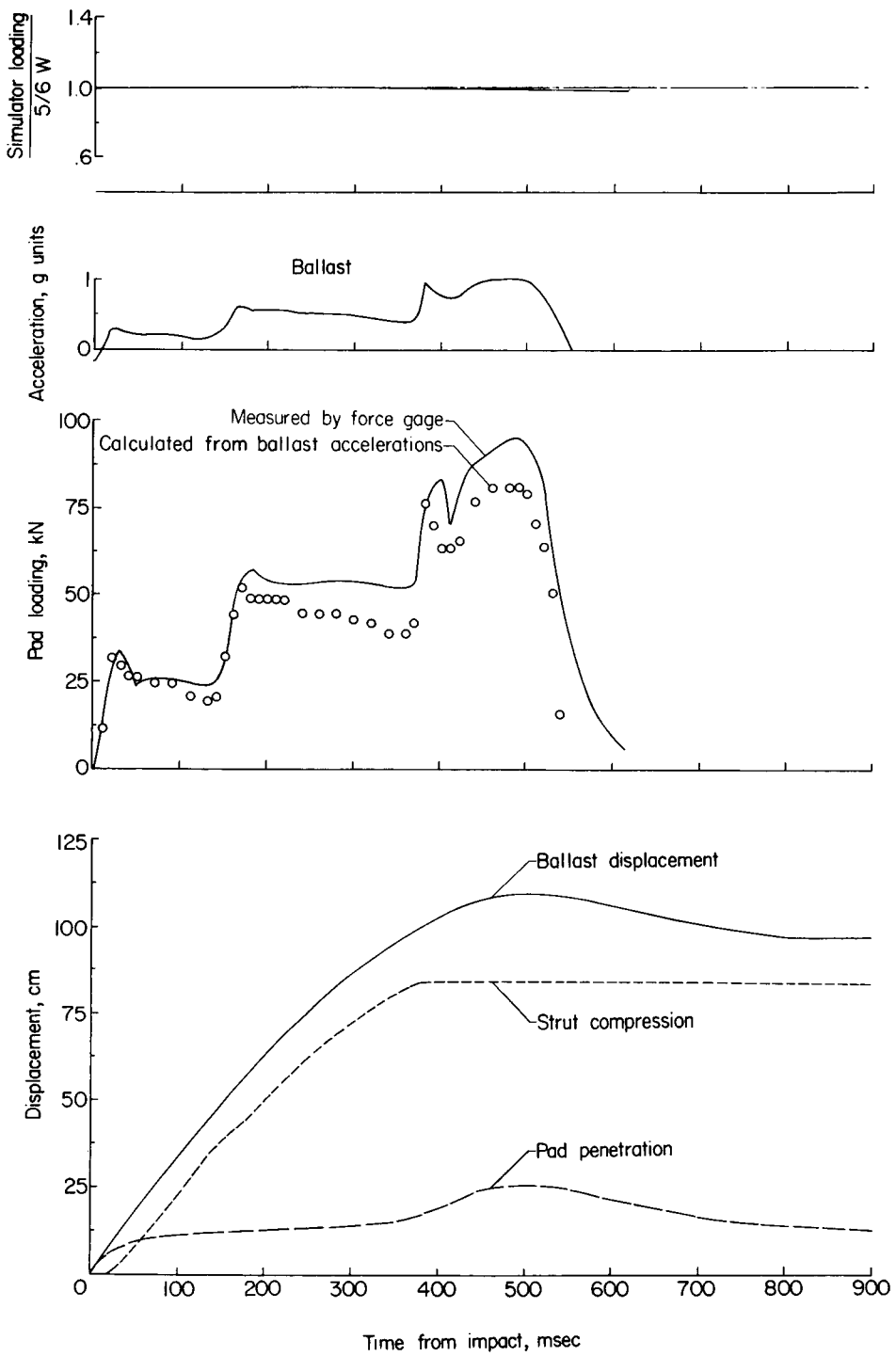

(x) Target, urethane foam; system mass, 6845 kg; impact velocity, 3.35 m/sec.

Figure 9.- Concluded.

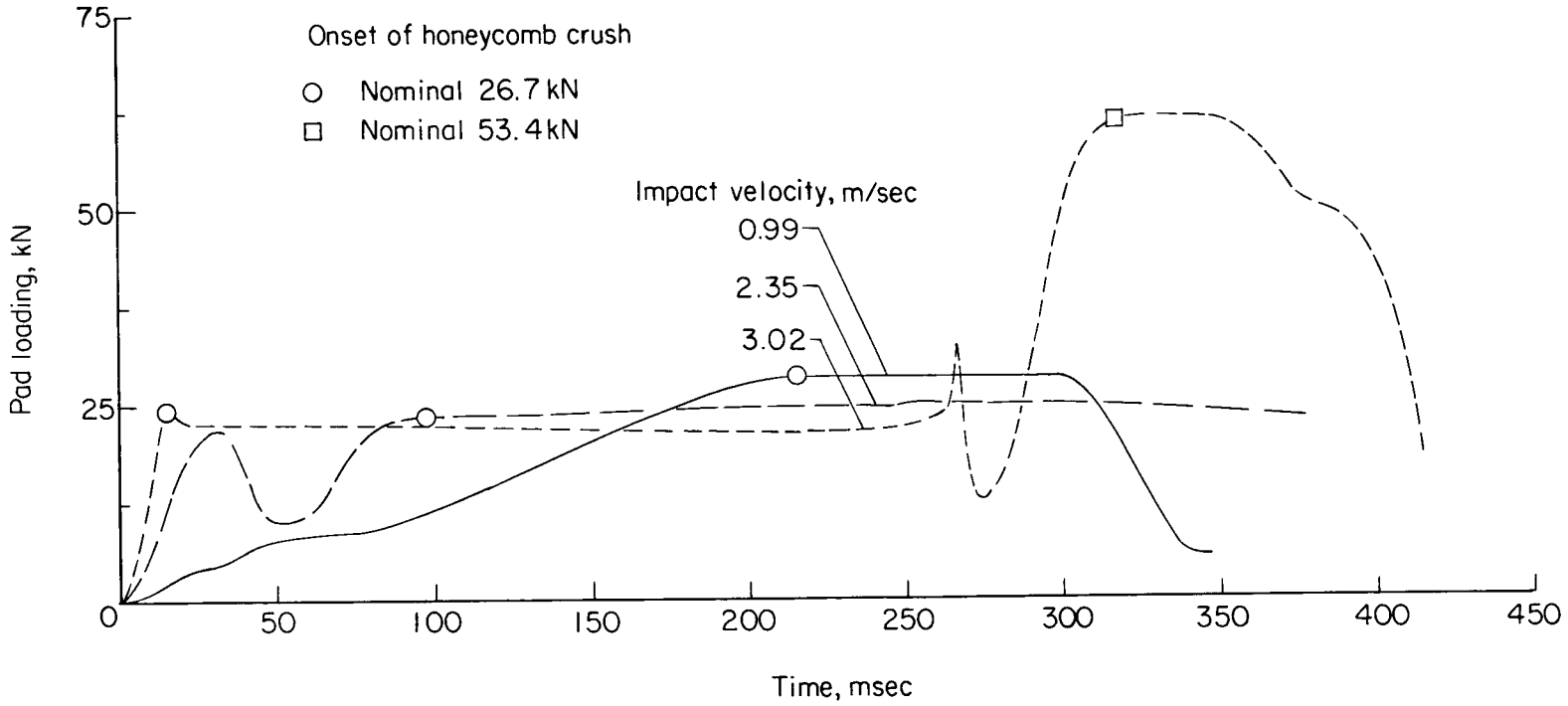

Figure 10.- Typical variation in pad loading time histories with impact velocity. Target, loosely packed Nevada 120 sand; system mass, 3506 kg.

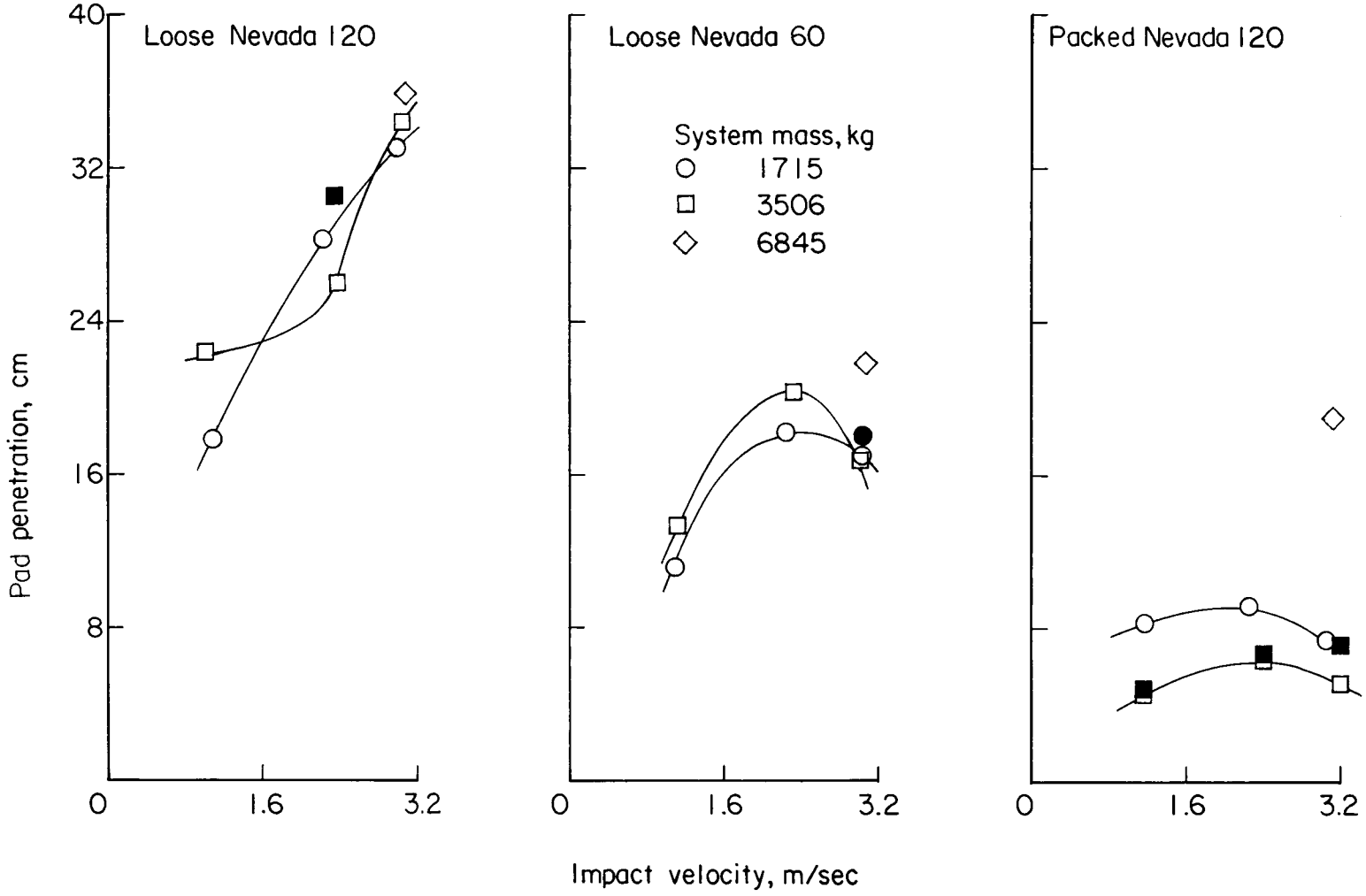

Figure 11.- Pad penetrations into granular test target materials. Open symbols refer to final penetration depths and solid symbols refer to maximum penetration prior to rebound.

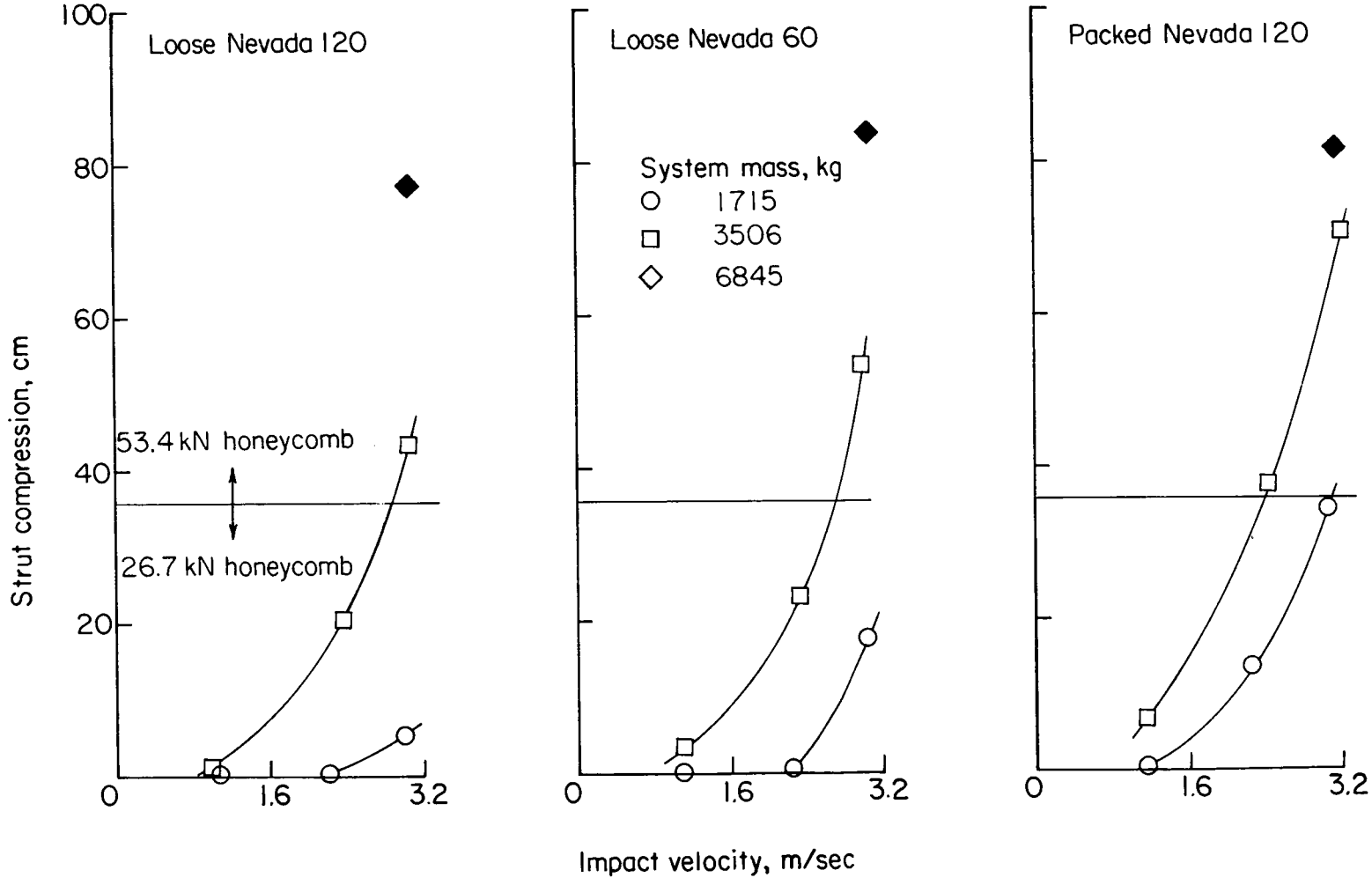

Figure 12.- Strut compression during impact with granular test target materials. Solid symbols indicate strut bottoming.

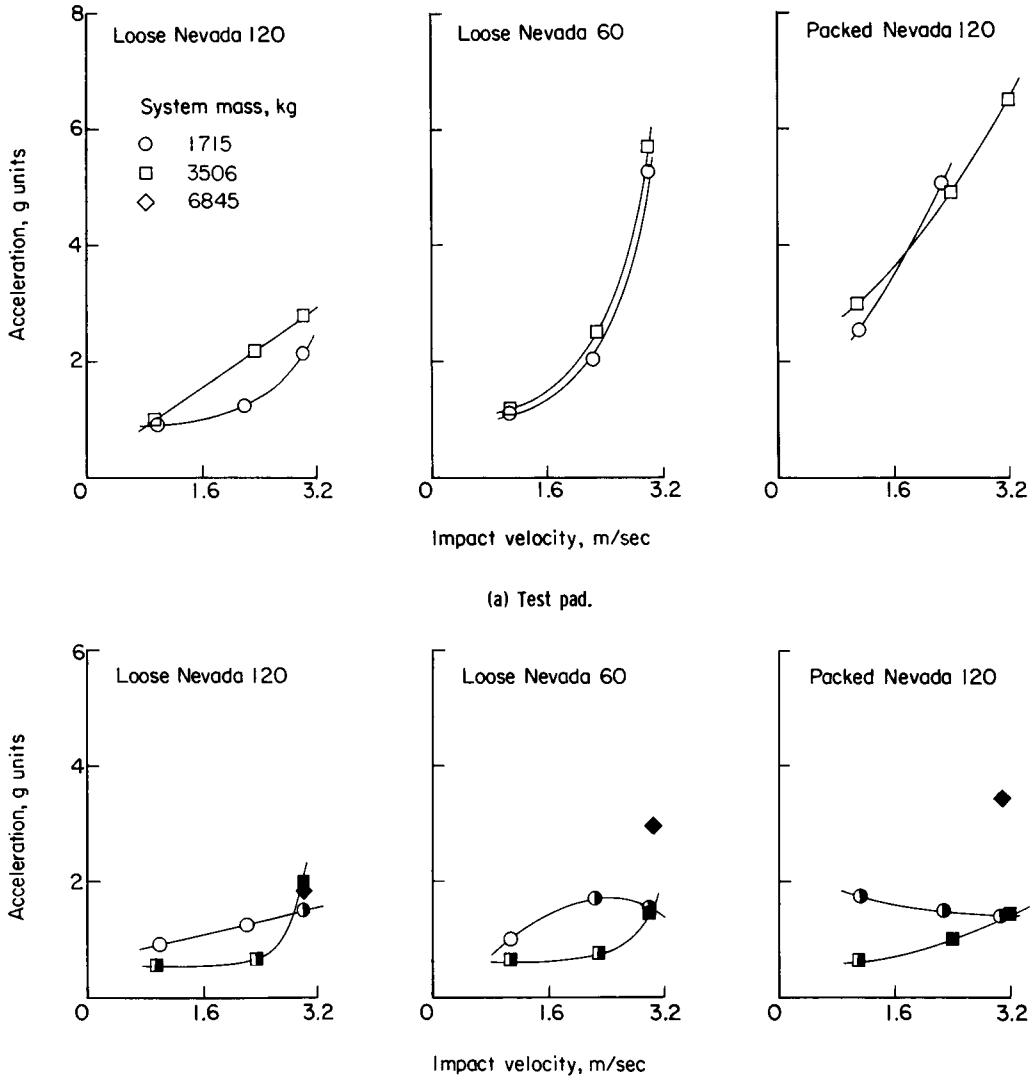

Figure 13.- Maximum pad and ballast accelerations incurred during impact with the sand target materials. In ballast data, open symbols refer to no strut compression; half-solid symbols refer to compression in 26.7-kN honeycomb cartridge; and solid symbols refer to compression in 53.4-kN honeycomb cartridge.

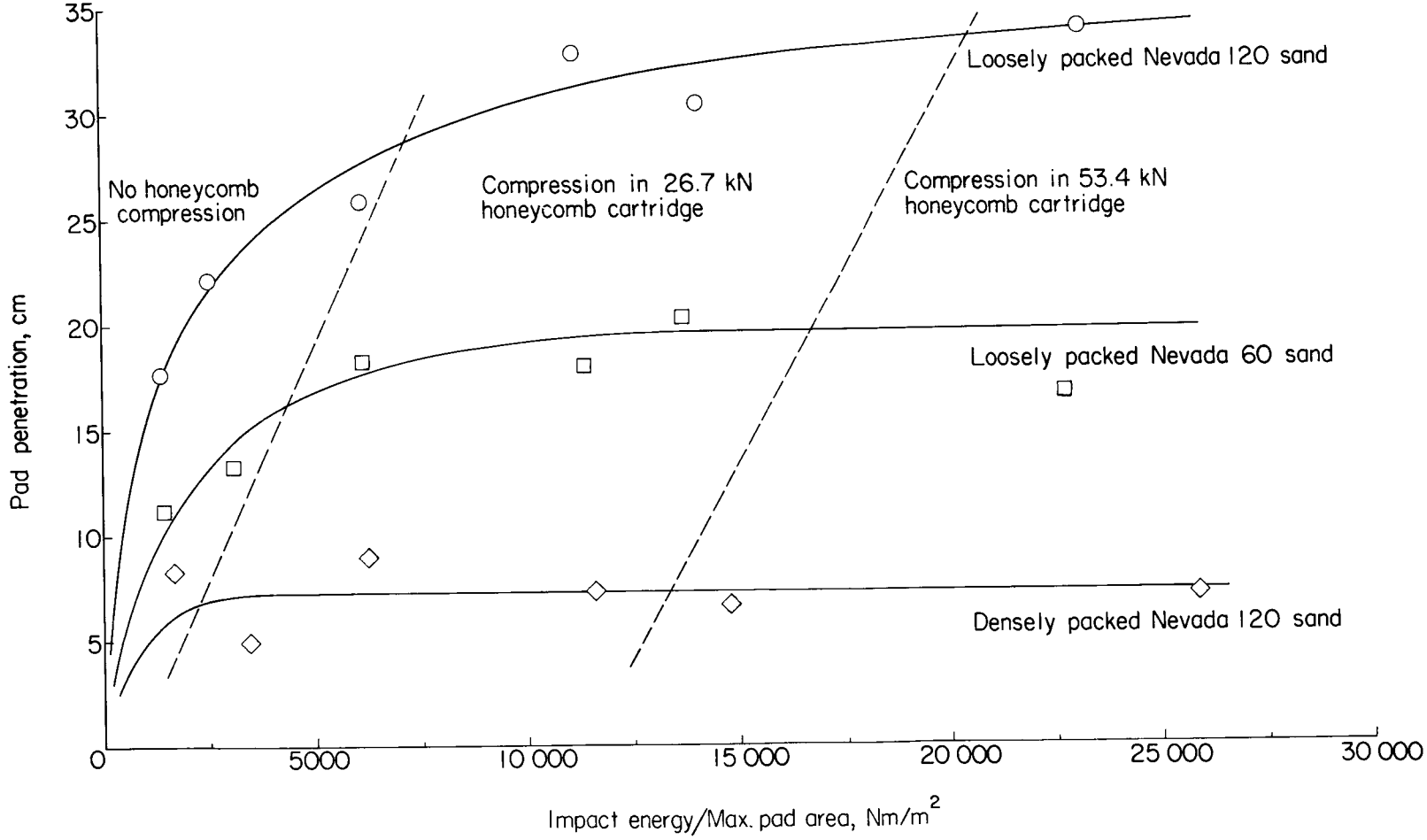

Figure 14.- Variation of pad penetration in particulate test target materials with system impact energy.

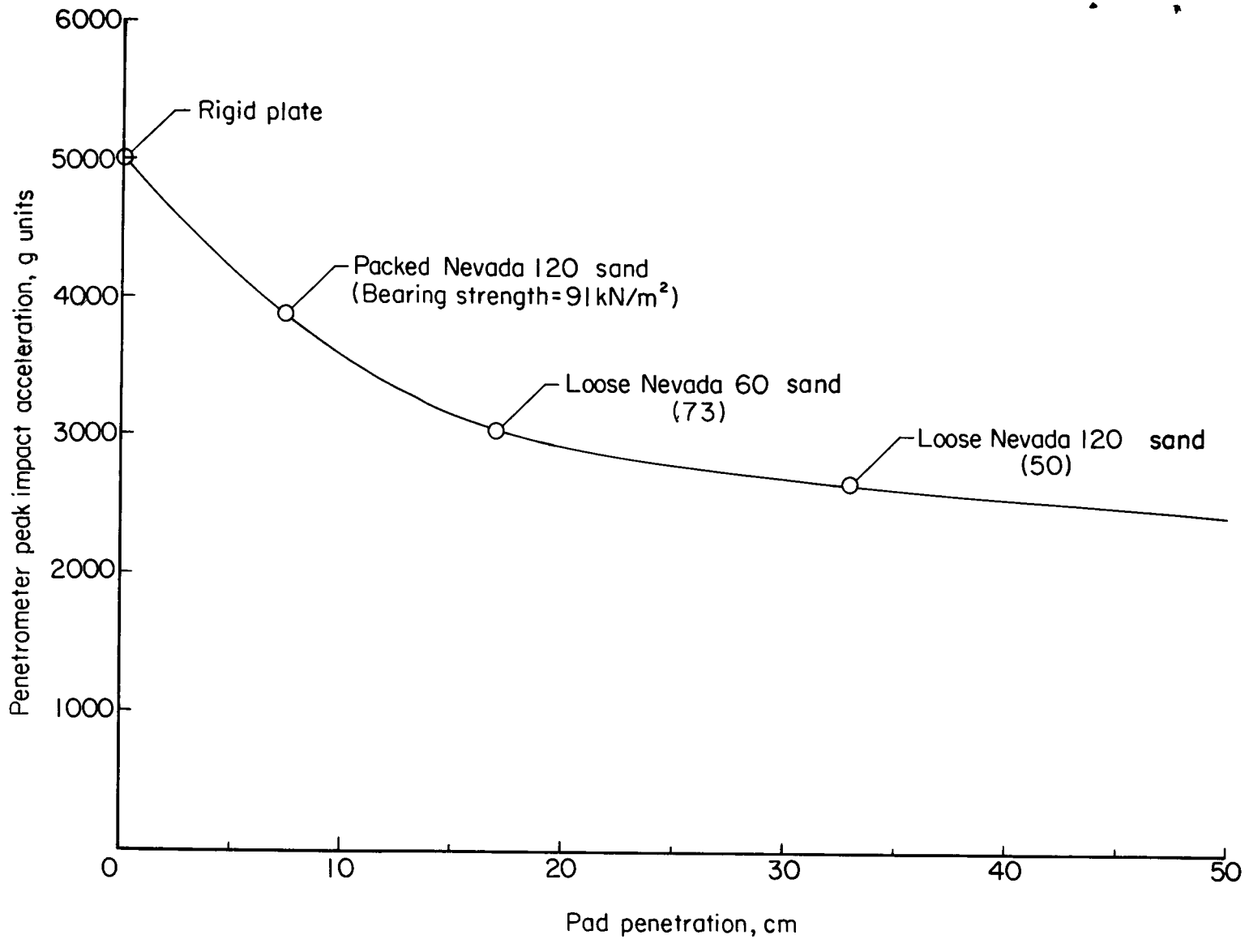

Figure 15.- Relationship between test landing gear pad penetrations and peak accelerations of an Apollo-oriented penetrometer impacting at approximately 46 m/sec. LM system mass, 1715 kg; impact velocity, 3.05 m/sec.